

Constraints of zircon Hf isotopes on ancient crustal reworking in the Early Paleozoic Altai accretionary wedge, Central Asian Orogenic Belt

Arnaud Broussolle^{a,b}, Yingde Jiang^{a,*}, Min Sun^b, Yang Yu^a, Jean Wong^b, Tan Shu^a, Kang Xu^a

^a State Key Laboratory of Isotope Geochemistry, Guangzhou Institute of Geochemistry, Chinese Academy of Sciences, 510640 Guangzhou, China

^b Department of Earth Sciences, the University of Hong Kong, Pokfulam Road, Hong Kong, China



ARTICLE INFO

Keywords:

Altai Orogenic Belt
Accretionary wedge
Magmatic reworking
Hafnium isotopes
Ancient crustal components

ABSTRACT

A debate exists on whether the deep crust of the Altai Orogenic Belt contains ancient crustal components. To further address this issue, geochemical analyses and zircon hafnium isotopic measurements were conducted on five Devonian magmatic rocks from the Southern Chinese Altai. Three volcanic rocks have rhyolitic compositions and two other intrusions have granite and granodiorite compositions, respectively. These samples all have calc-alkaline, peraluminous compositions and “arc-related” trace element signatures, marked by enrichment in large-ion lithophile elements relative to many of the high field strength elements. Hf-in-zircon isotopic data for these rocks show variable $\varepsilon_{\text{Hf}}(t)$ values ranging from -25 to $+5$, with corresponding T_{DM}^{c} model ages varying from ca. 2.7 to ca. 0.9 Ga. These findings represent the first report describing negative zircon $\varepsilon_{\text{Hf}}(t)$ values for the Devonian magmatic rocks of the region, documenting magmatic reworking of ancient crustal components. The very similar trace elemental patterns and indistinguishable zircon Hf isotopic characteristics, between the studied magmatic rocks and the pre-existing Ordovician accretionary wedge sediments (the Habahe Group), supports the notion that the magmatic rocks are derived from magmatic reworking of the wedge that contains ancient crustal components. The studied magmatism is synchronous with Middle Devonian anatexis of the Ordovician wedge at low-pressure/high-temperature conditions and extrusion of bimodal volcanic rocks occurred in Devonian extensional basins. These events have been collectively taken as proxies of Devonian lithospheric extension in the Chinese Altai. Integrated mapping of Hf isotopic data for the bulk S-type Devonian magmatism of the Chinese Altai shows different domains with dissimilar Hf isotopic signatures. This further indicates that the magma source, i.e., the Ordovician wedge, is compositionally heterogeneous and contains ancient crustal components.

1. Introduction

Accretionary orogens represent major sites of growth of continental lithosphere through long-lasting, continuous subduction of oceanic crust, as best exemplified by modern western Pacific convergent margins (Cawood and Buchan, 2007; Cawood et al., 2009; Kemp et al., 2009). Prolonged accretion brings diverse geological units together, including both oceanic stratigraphic units scraped off the down-going oceanic crust and geochemically evolved crustal components from the upper plate continental crust via sedimentary additions or tectonic erosion (e.g., Kusky et al., 2013; Safonova, 2017; Stern, 2011). This process accounts for the generation of giant and chemically heterogeneous sedimentary wedges representing a key structure of accretionary systems worldwide (Collins and Richards, 2008; Gray and Foster, 2004; Jiang et al., 2017; Long et al., 2008; Weinberg et al.,

2018). While variable lithological units have been well mapped out and clarified in a number of modern and fossil accretionary systems (Safonova and Santosh, 2014 and references therein), such elucidation is not straightforward for seriously deformed and metamorphosed accretionary wedges, and quite often, geochemical analysis may provide crucial evidence (e.g., Huang et al., 2020a; Kemp et al., 2009; Long et al., 2012).

In the Central Asian Orogenic Belt (CAOB), the largest known Phanerozoic accretionary system on earth (Mossakovskiy et al., 1993; Sengör et al., 1993; Windley et al., 2007; Xiao et al., 2015a), the Altai accretionary wedge developed at the active margin of the Tuva-Mongolian continental blocks in early Paleozoic time (Jiang et al., 2019; Soejono et al., 2018). It has not only accommodated fragments of oceanic affinity from the south but also received detritus from the newly developed arc system as well as the continental blocks in the

* Corresponding author.

E-mail address: jiangyd@gig.ac.cn (Y. Jiang).

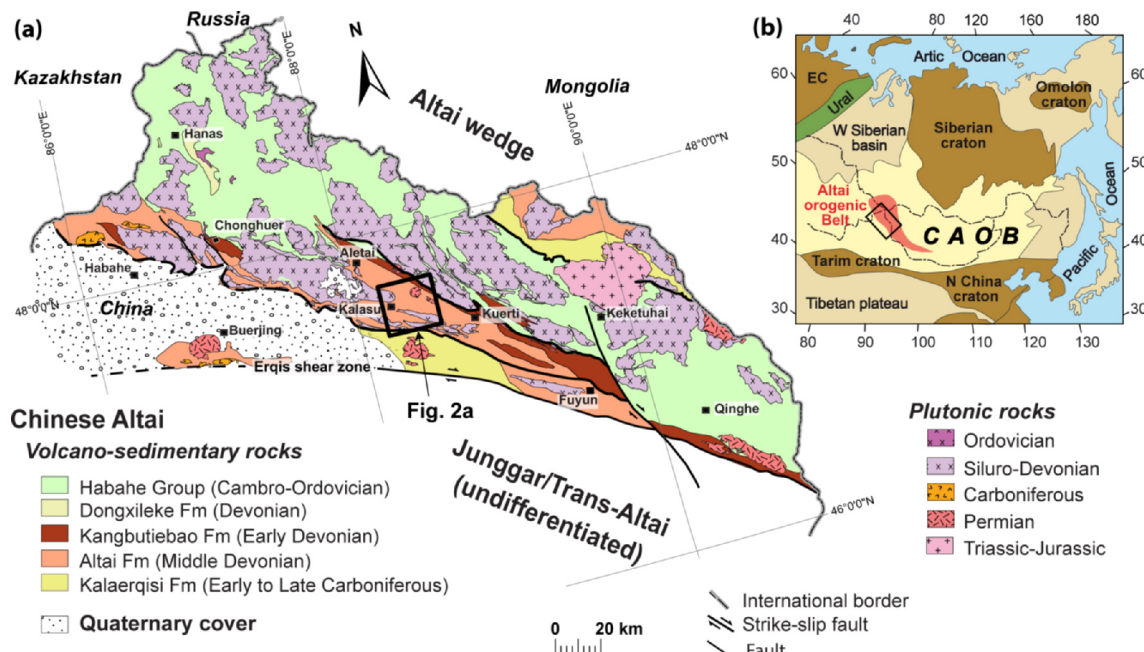


Fig. 1. Generalized geological map of the Chinese Altai showing the different lithostratigraphic units and magmatism (modified after Broussolle et al. (2019)). The study area is outlined (Fig. 2a). The upper right inset shows the extension of the Central Asian Orogenic Belt (CAOB), the location of the Altai orogenic Belt (outlined by red shading) and the Chinese Altai (delineated by small square) (modified after Jahn et al. (2000)). EC: Eastern European craton. (For interpretation of the references to colour in this figure legend, the reader is referred to the web version of this article.)

north (Broussolle et al., 2019; Chen et al., 2014; Jiang et al., 2011). The occurrence of oceanic lithological units was already mapped out in many places (Safonova et al., 2004; Xiao et al., 2009), but the identification of evolved continental components, especially ancient ones, are not straightforward, because of strong deformation and high-grade metamorphism of the wedge. The understanding of the crustal architecture of the Altai wedge is therefore a difficult task. The Chinese Altai, representing the Chinese segment of the Altai wedge, underwent prominent multiphase Devonian and Permian tectono-thermal events, resulting in greenschist- to granulite-facies metamorphism (Broussolle et al., 2019; Jiang et al., 2015, 2019). The high-grade rocks were previously interpreted as the Precambrian continental basement, but recent studies revealed that the detrital zircons mostly have early Paleozoic ages (e.g., Broussolle et al., 2018; Jiang et al., 2011; Sun et al., 2008; Zhang et al., 2015). Geochemical and geochronological investigations further suggested that the high-grade rocks are metamorphosed equivalents of the Ordovician accretionary wedge sediments, suggesting that the existence of Precambrian basement in the Altai orogen is highly speculative (Chen et al., 2014; Jiang et al., 2017; Long et al., 2007, 2012).

Although the original sedimentary features were already erased by later tectono-thermal events, the existence of both Paleozoic and Precambrian detrital zircons in the wedge sediments implies sedimentary provenance including both newly-formed and much-evolved crustal components (e.g., Jiang et al., 2011; Long et al., 2007; Sun et al., 2008; Wang et al., 2014b; Zhang et al., 2017a). Notably, nearly half of the detrital zircons in the Chinese Altai wedge sediments are characterized by positive $\epsilon_{\text{Hf}}(\text{t})$ values and nearly all igneous zircons from the bulk Paleozoic granitoids in the region have positive zircon $\epsilon_{\text{Hf}}(\text{t})$ values (Cai et al., 2011b, 2012; He et al., 2018; Luo et al., 2018; Song et al., 2019; Sun et al., 2009; Wang et al., 2011; Zhang et al., 2017a; Zheng et al., 2016). These features led many authors to suggest that the Chinese Altai consists predominantly of juvenile components. In contrast, many Ordovician metasedimentary rocks and Paleozoic granitoids have negative whole-rock $\epsilon_{\text{Nd}}(\text{t})$ values (Chen and Jahn, 2002; Hu et al., 2000; Jiang et al., 2016; Long et al., 2012; Wang et al., 2014b). While the negative whole-rock $\epsilon_{\text{Nd}}(\text{t})$ data were taken as a clue for the

existence of ancient crustal components (Song et al., 2019; Wang et al., 2006, 2009a; Zhang et al., 2017b), others believed that metasomatism in the magma source may have affected Nd, but not Hf isotopic system, leading to decoupled Nd and Hf isotopic systems in the region (Yu et al., 2017). These uncertainties are responsible for a range of contradictory models of the nature of the Chinese Altai (Broussolle et al., 2019; Jiang et al. 2016; Song et al., 2019; Wang et al., 2009a, 2009b; Yu et al., 2017) which hinders our understanding of the crustal evolution of the region.

The Kalasu area located in the center of the Chinese Altai is characterized by the occurrence of a significant number of gneissic granitoids and felsic volcanic rocks. These rocks were traditionally thought to be the product of arc magmatism (Cai et al., 2011b; Chai et al., 2009; Yang et al., 2011). However, recent investigations indicated a close temporal and spatial link between the emplacement of the granitoids and anatexis in the deep crust, which suggested a S-type affinity for the granitoids (Broussolle et al., 2018; Jiang et al., 2016). The geochemical signatures of the granitoids hence have a great potential for investigation of the compositional characteristics of the deep crust. In this paper, we report the first systematic negative/mixed $\epsilon_{\text{Hf}}(\text{t})$ signatures for the Devonian felsic magmatic rocks in the region, implying magmatic reworking of ancient crustal components. Whole-rock geochemical analysis further supports the notion that the granitoids and their eruptive equivalents derived from the Ordovician wedge. In addition, combined with regional published data, our results suggest a compositionally heterogeneous crustal nature for the Altai accretionary wedge, which represents a common characteristic of accretionary wedges worldwide (e.g., Augustsson et al., 2016; Gray and Foster, 2004; Kemp et al., 2009).

2. Geological setting

2.1. Overview of the Chinese Altai

The CAOB, extending from the Siberian Craton in the north to the Tarim and North China cratons in the south, has an evolutionary history from ca. 850 to 230 Ma (Fig. 1b) (Jahn et al., 2000; Mossakovskiy et al., 1993; Schulmann and Paterson, 2011; Şengör et al., 2018; Windley

et al., 2007; Xiao et al., 2015b; Zhao et al., 2018). According to Xiao et al. (2015b), the CAOB is composed of three main collage systems, i.e., the Kazakhstan Collage in the west, the Tarim-North China Collage in the south and the Mongolian Collage in the east. On one hand, they have comparable lithological components consisting of Paleozoic accretionary prisms, cratonic terranes, Paleozoic oceanic domains and Neo-Proterozoic to Paleozoic arcs (Rojas-Agramonte et al., 2011; Şengör et al., 2018; Wilhem et al., 2012; Xiao et al., 2015b; Zhao et al., 2018). On the other hand, they exhibit contrasting geodynamic evolution during the Paleozoic prior to their amalgamation during the assembly of the supercontinent Pangea in the Permian to Early Triassic (e.g., Şengör et al., 2018; Wilhem et al., 2012; Xiao et al., 2015b; Zhao et al., 2018).

The ~2000 km Ordovician Altai accretionary wedge extends from Kazakhstan and Russia in the northwest, through NW China, to Mongolia in the East (Fig. 1a, b) (Jiang et al., 2017; Li et al., 2019; Long et al., 2010; Soejono et al., 2018). This wedge was developed on the active margin of the Cambro-Ordovician Ikh-Mongol arc system that in turn developed on the Tuva-Mongol continental ribbons further north (Broussolle et al., 2019; Janoušek et al., 2018; Jiang et al., 2017). The Altai wedge is composed of a thick greywacke-dominated sequence, known as the Habahe Group in the Chinese segment (Jiang et al., 2016, 2017). The Habahe Group was affected by extensive Late Siluro-Devonian magmatism, deformation and metamorphism, leading to transformation of the sedimentary wedge into mature orogenic crust (Burenjargal et al., 2014; Cai et al., 2011b, 2012; Jahn et al., 2000; Jiang et al., 2016; Liu et al., 2012; Sun et al., 2009; Wang et al., 2009a; Yuan et al., 2007).

The Chinese Altai was further affected by a less extensive Permian shortening, resulting in numerous NW-SE-trending upright folds and the formation of heterogeneous NW-SE-trending subvertical high temperature deformation zones along the southern flank (Broussolle et al., 2018, 2019). High-temperature/low-pressure (HT/LP) metamorphic assemblages were found to develop in association with this event (e.g., Jiang et al., 2019; Liu et al., 2020; Wei et al., 2007). U-Pb zircon dating from these zones yielded metamorphic ages ranging from 300 to 260 Ma (Li et al., 2014; Liu et al., 2020; Tong et al., 2014; Wang et al., 2009b, 2014a; Zheng et al., 2007). This event was considered as a response to amalgamation between the Chinese Altai and its southerly Junggar arc domain during the Early Permian (Broussolle et al., 2018; Jiang et al., 2019; Li et al., 2017).

2.2. Geology of the Kalasu area

The Kalasu area is located in the Southern Chinese Altai (Figs. 1 and 2a). The oldest sequence in the region is the Ordovician Habahe Group (Fig. 2b). This group is originally composed of greywacke-dominated clastic to volcano-clastic sedimentary rocks (Broussolle et al., 2018; Long et al., 2007). Detrital zircons from the Habahe Group show age peaks in a range between 500 and 485 Ma (Broussolle et al., 2018; Jiang et al., 2011; Long et al., 2007; Yang et al., 2011). The Habahe Group is variably metamorphosed up to granulite-facies. In the study area, it occurs as un-molten paragneiss and schist in the south and as stromatic to nebulitic migmatite, forming alternating metatexite-dominated and diatexite-dominated domains in the central part (Figs. 2a and 3f). Metamorphic zircons from the migmatites as well as igneous zircons from leucosomes yielded U-Pb ages ranging from 400 to 380 Ma (Broussolle et al., 2018; Jiang et al., 2010; Long et al., 2007), synchronous with the formation of granitoids and felsic volcanic rocks in the region. The Habahe Group was unconformably overlain by a thick Devonian sequence of volcanoclastic and tuff, namely the Kangbutiebao Formation (BGMRX, 1978). Volcanic rocks from this formation yielded U-Pb ages between 412 and 395 Ma (Figs. 2a, b and 3a-b) (Table 3; Broussolle et al., 2018 and references therein). The Kangbutiebao Formation is further overlain by the Altai Formation composed of low-grade biotite schist interlayered with metarhyolite and minor

marble (Figs. 2a, b and 3c). A metarhyolite from this formation yielded U-Pb age at ca. 388 Ma, documenting a Middle Devonian age for the sequence (Figs. 2a, b and 3c) (Broussolle et al., 2018).

The region was intruded by a large number of 412–368 Ma granitoids associated with minor gabbros, all of which are elongated NW-SE and gneissified (Fig. 2a) (Broussolle et al., 2018; Cai et al., 2011b; Yang et al., 2011). The less extensive Permian magmatic rocks are weakly deformed and show elongated and/or circular shape (Fig. 2a) (Lin et al., 2019; Liu et al., 2018; Windley et al., 2002). The study area was affected by both Devonian and Permian tectono-metamorphism cycles. The Devonian cycle corresponds to an Early Devonian medium-pressure/medium temperature (MP-MT) metamorphic phase followed by a Middle Devonian extension-induced HT-LP metamorphic one and ended with a Late Devonian WNW-ESE shortening (Broussolle et al., 2018). The Permian cycle is characterized by amphibolite- to granulite-facies (HT-LP) metamorphism formed due to the NNE-SSW convergence between the Chinese Altai and the Junggar arc domain (Broussolle et al., 2018, 2019; Jiang et al., 2019; Li et al., 2017; Zhang et al., 2015). The interference between the two orthogonal orogenic cycles resulted in juxtaposition of vertical zones with distinct high- and low-grade metamorphism which were also imaged by recent geophysical analysis (Guy et al., 2020).

Based on the heterogeneous metamorphism mentioned above, Broussolle et al. (2018) described the Kalasu area (Fig. 2a) as 1) orogenic upper crust in the north, composed of greenschist-facies Devonian felsic metavolcanic rocks and metasediments, 2) orogenic middle crust in the south, composed of greenschist- up to amphibolite-facies paragneisses and orthogneisses, and 3) orogenic lower crust in the center, composed of amphibolite to granulite-facies paragneisses, orthogneisses and migmatites. Given that the Devonian metavolcanic rocks resemble the Devonian granitoids in terms of their ages and chemical characteristics, the metavolcanics could be considered as the extrusive equivalents of the gneissic granitoids (Figs. 2a and 3a-e).

3. Petrography of the magmatic rocks

In this study, five felsic magmatic rocks were studied, including two granitoids and three volcanic rocks. Their detailed descriptions of petrography as well as their zircon U-Pb ages are presented in detail in Broussolle et al. (2018). Here, their key petrographic features are briefly summarized. The three metavolcanic rocks were collected from the orogenic upper crust segment in the north (Table 1). These samples show a weak foliation on the outcrops (Fig. 3a-c). Among them, sample 15AT254-1 is a fine-grained metatuff composed mainly of plagioclase, quartz and muscovite with minor biotite, ilmenite and tourmaline (Fig. 4a). The muscovite and scarce biotite define a gently folded foliation. Sample 15AT245-1 is a medium-grained metavolcano-clastic rock consisting of elongated porphyroclasts of quartz and feldspar with oriented biotite, recrystallized bands of quartz, plagioclase and weakly oriented muscovite (Fig. 4b). Less commonly, calcite occurs in some feldspar porphyroclasts (inset in Fig. 4b). Sample 16A2-1 is a metarhyolite that is interlayered within metapelitic rocks in outcrop (Fig. 3c). This sample is composed of quartz, plagioclase, biotite and scarce muscovite and garnet porphyroblasts with numerous quartz inclusions (Fig. 4c). The granitic sample 16A10-1 was collected from a kilometric scale body in the orogenic middle crust in the south and shows gneissic structure and underwent medium grade metamorphism (Fig. 3d). This sample is composed of recrystallized plagioclase, quartz, K-feldspar, biotite and muscovite which define a strong foliation (Fig. 4d). The sample 15AT100-2, collected from the central domain of the orogenic lower crust, is a gneissic granitoid emplaced within the Habahe Group and underwent high-grade metamorphism (Broussolle et al., 2018) (Fig. 3e). The sample is composed of plagioclase, quartz, K-feldspar and biotite, with accessory minerals of zircon, ilmenite and magnetite (Fig. 4e). Previous geochronological studies revealed that both the granitoids and the metavolcanic rocks have zircon U-Pb ages

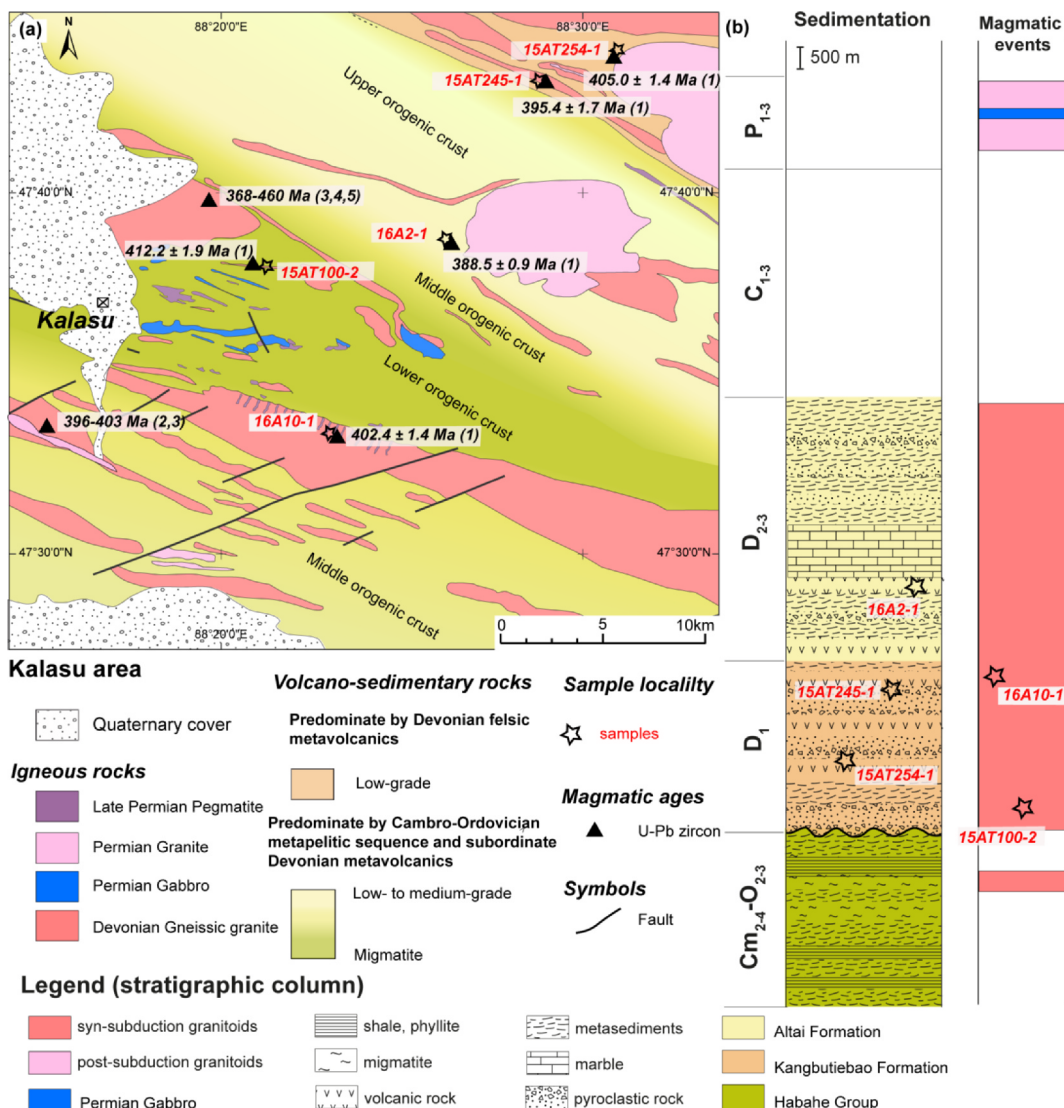


Fig. 2. (a) Lithological map of the Kalasu area, located in the Southern Chinese Altai showing the distribution of the different magmatic rocks. The locations of the samples and previous magmatic zircon U-Pb ages are shown. Data sources: [1] Broussolle et al. (2018); [2] Yang et al. (2011); [3] Cai et al. (2011b); [4] Yuan et al. (2007) and [5] Wang et al. (2006). See text for explanation. (b) Stratigraphic column showing different sequences in the Kalasu area and the related magmatic events (after Broussolle et al. (2019)).

ranging from 412 to 388 Ma (Broussolle et al., 2018), coeval with the Middle Devonian high-temperature event in the region (Long et al., 2007; Jiang et al., 2010). Besides, these felsic magmatic rocks usually contain Cambro-Ordovician inherited zircons (Fig. 7a-e; e.g., sample 15AT148-2 in Broussolle et al. (2018)), similar to the most common age of the detrital zircons from the surrounding Habahe Group.

4. Analytical methods

4.1. Whole-rock geochemistry

Approximately 5 kilos of samples were carefully selected for powder and zircon separation. Sample preparation, LOI and whole-rock major analyses were then performed at the Department of Earth Sciences, The University of Hong Kong (HKU), China with methods similar to that described in Yuan et al. (2007). Major elements of selected whole-rock samples were determined with a Philips PW2400 wavelength-dispersive X-ray fluorescence spectrometer (WD-XRFS) on fused glass disks at HKU. The analytical errors are about 1–2% for SiO₂, Al₂O₃, TiO₂, Fe₂O₃ and MgO and ≤3% for other oxides.

Trace-element analyses were performed at the State Key Laboratory

of Isotope Geochemistry (SKLaBIG), Guangzhou Institute of Geochemistry, Chinese Academy of Sciences (GIG-CAS). A Perkin-Elmer Sciex ELAN 6000 inductively coupled plasma-mass spectrometry (ICP-MS) after acid digestion of samples in high-pressure Teflon vessels according to the detailed procedures described by Li et al. (2006). The USGS and Chinese National standards AGV-2, GSR-1, GSR-2, MRG-1, BCR-1, W-2 and G-2 were used for calibrating element concentrations of the analyzed samples. Analytical precisions for REE and other incompatible element analyses are typically 1–2%. Whole-rock major and trace elements data are given in Table 1 and are plotted using the Geochemical package of GCDkit (Janoušek et al., 2006).

4.2. Zircon Hf isotopic analysis

Zircons from the studied samples were already analyzed for U-Pb ages and results were reported in Broussolle et al. (2018). Zircon CL images were performed by a JEOL microprobe installed at the SKLaBIG, GIG-CAS. In this study, zircon Hf isotopic analyses were further performed on selected igneous zircon grains using a Nu plasma HR MC-ICP-MS coupled with a 193 nm excimer laser ablation system at HKU. A beam spot of 55 μm was used for each analysis on the same position as

Table 1

Whole-rock major- and trace-element compositions of the magmatic rocks from the Kalasu area, SW Altai Orogenic Belt.

Samples Rock-type	15AT254-1 metatuff	15AT245-1 metavolcano-clastic	16A2-1 metarhyolite	16A10-1 gneisic granite	15AT100-2 gneisic granodiorite
Age (Ma)	405.0 ± 1.4	395.4 ± 1.7	388.5 ± 0.9	402.4 ± 1.4	412.2 ± 1.9
Longitude	88.518	88.479	88.446	88.375	88.337
Latitude	47.734	47.721	47.654	47.555	47.634
SiO ₂	72.49	70.43	77.60	76.36	67.14
TiO ₂	0.43	0.41	0.23	0.10	0.80
Al ₂ O ₃	12.31	13.81	11.63	12.60	15.47
FeO _T	3.71	3.36	1.72	1.49	5.35
MnO	0.03	0.09	0.08	0.03	0.07
MgO	3.63	0.69	0.33	0.38	1.64
CaO	0.41	1.59	1.03	0.41	3.70
Na ₂ O	0.62	2.94	3.14	2.77	3.13
K ₂ O	6.02	5.40	3.04	3.82	1.82
P ₂ O ₅	0.10	0.09	0.07	0.04	0.24
LOI	0.94	1.02	0.94	0.93	0.33
Total	100.70	99.83	99.81	98.94	99.69
Sc	11.23	15.83	6.54	16.99	16.44
V	32.32	21.35	11.88	5.19	81.33
Cr	5.36	3.03	4.50	3.29	17.29
Co	4.01	1.56	1.01	0.84	9.65
Ni	3.61	2.59	2.89	2.17	11.27
Ga	15.89	17.28	13.84	19.35	18.39
Cs	6.30	1.93	2.85	7.01	3.10
Rb	222.60	173.00	127.50	206.60	74.38
Ba	450.90	520.40	886.80	415.70	390.20
Th	9.37	8.58	9.17	9.07	0.27
U	3.16	2.49	1.46	1.96	0.66
Pb	2.12	2.94	12.75	13.03	10.02
Nb	10.29	9.97	8.37	20.19	6.69
Ta	0.69	0.67	0.61	1.23	0.41
Sr	31.83	33.68	42.59	48.23	172.90
Y	92.54	35.76	48.62	51.15	16.63
Zr	236.50	199.60	149.70	69.63	157.80
Hf	6.63	5.63	5.01	3.10	4.25
La	142.30	22.33	23.72	10.27	7.25
Ce	294.00	48.99	49.99	33.28	17.62
Pr	34.56	6.29	6.68	3.03	2.51
Nd	135.30	26.10	26.75	12.08	12.96
Sm	27.89	5.70	5.76	3.31	3.61
Eu	4.44	1.49	0.98	0.54	1.46
Gd	24.91	5.56	5.74	4.74	3.82
Tb	3.37	0.93	1.07	1.08	0.62
Dy	16.81	5.82	7.19	7.63	3.57
Ho	2.94	1.26	1.60	1.70	0.68
Er	7.61	3.73	4.89	4.89	1.66
Tm	1.03	0.57	0.78	0.77	0.20
Yb	6.45	3.67	5.17	5.04	1.10
Lu	0.97	0.57	0.79	0.76	0.16
Ti	2669.00	2585.80	1308.70	548.70	4743.80
Mn	217.40	708.20	592.30	222.00	548.10
Cu	2.73	1.79	3.59	1.03	18.93
Zn	23.27	32.04	80.69	24.21	72.47
Ge	4.12	2.05	1.82	1.62	2.02
Eu*	0.51	0.81	0.52	0.42	1.2
La _N /Yb _N	15.02	4.14	3.12	1.39	4.5
SumREE	702.59	133.01	141.11	89.12	57.2

the previous U-Pb spot. All Hf isotopic data were calculated with the decay constant of $1.865 \times 10^{-11} \text{ yr}^{-1}$ reported by Scherer et al. (2001). The chondritic values of $^{176}\text{Lu}/^{177}\text{Hf}$ (CHUR, today) = 0.0332 and $^{176}\text{Hf}/^{177}\text{Hf}$ (CHUR, today) = 0.282772 reported by Blichert-Toft and Albarède. (1997) were used for the calculation of $\epsilon_{\text{Hf}}(t)$ values. The values for the depleted mantle (DM) reported by Griffin et al. (2000) were used to define the DM evolution line (i.e., present-day $^{176}\text{Hf}/^{177}\text{Hf}$ = 0.28323 and $^{176}\text{Lu}/^{177}\text{Hf}$ = 0.0384). Given that zircons are generally formed in granitic magma derived from felsic crust, a “crust” model age (T_{DM}^{C}) is more meaningful than depleted mantle model age (Griffin et al., 2002). Further details of the methodology can be found in Kröner et al. (2014). The Hf isotopic data are listed in Table 2.

5. Results

5.1. Geochemistry

The metavolcanic rocks have high SiO₂ (70.40–77.60 wt%) and K₂O (3.04–6.02 wt%) and low TiO₂ (0.23–0.43 wt%) and Al₂O₃ (11.60–13.80 wt%) contents (Table 1). They fall in the rhyolite field on the SiO₂ versus Na₂O + K₂O diagram (Le Bas et al., 1986) (Fig. 5a, Table 1). They are strongly peraluminous with high A/CNK values (1.05–1.51). On the Chondrite normalized diagram, they show LREE enrichment ($[\text{La}/\text{Yb}]_{\text{N}} = 3.12\text{--}15.0$) and intermediately negative Eu anomalies ($\text{Eu}/\text{Eu}^* = 0.51\text{--}0.81$; Fig. 6a). On the primitive mantle normalized diagram, these samples display enrichment of large-ion lithophile elements (LILE) (Ba, Rb, Th and U) relative to many of the high

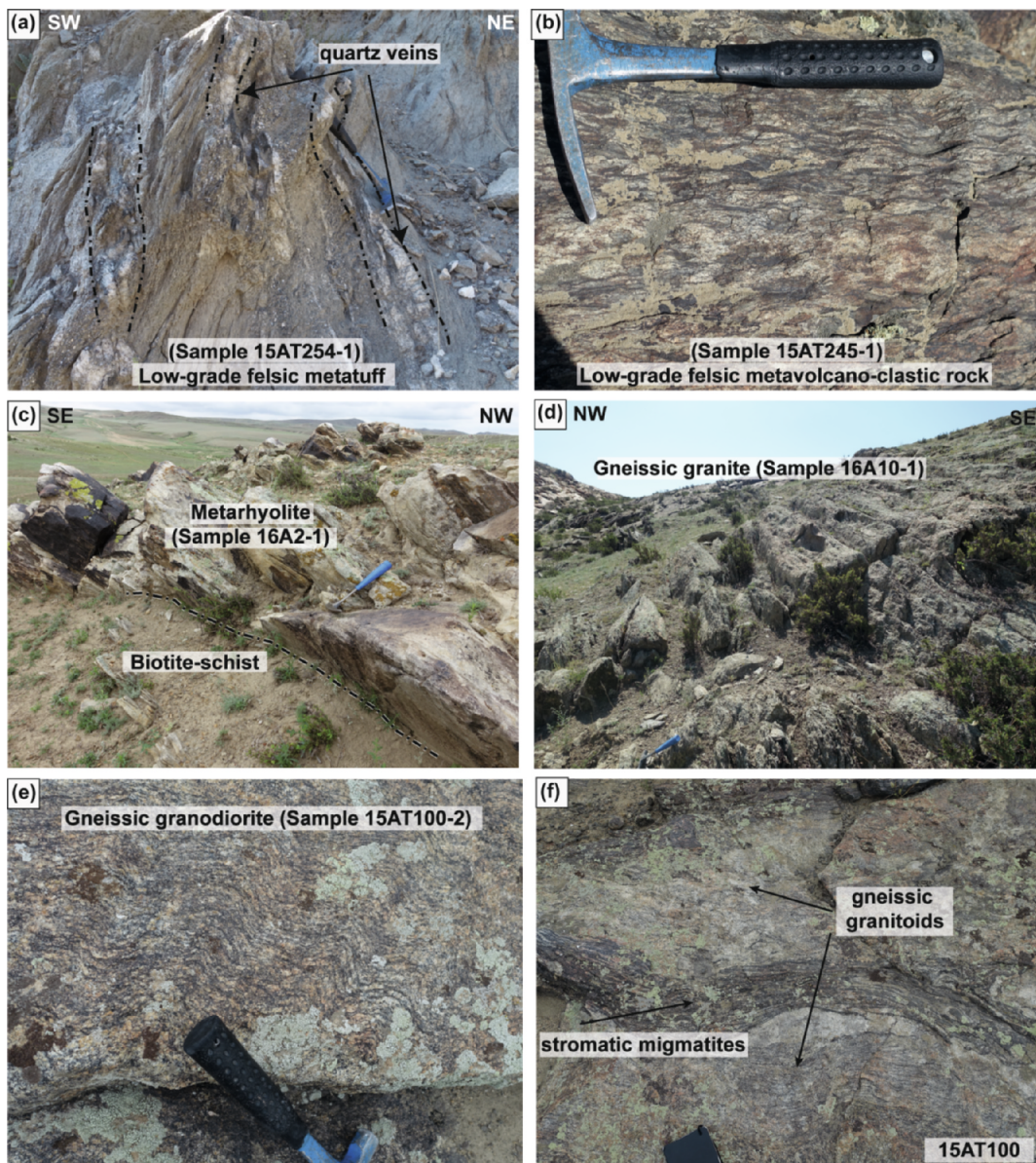


Fig. 3. Field photographs of magmatic rocks from the Kalasu area. (a), (b) and (c) show meta-volcanic rocks from the north upper orogenic crust; (d) and (e) represent two gneissic granitoids intruded the Habahe Group in the central part and in the south, corresponding to orogenic lower and middle crust, respectively. (f) Field photograph illustrating partial melting of the Habahe Group forming diatexite in the central domain.

field strength elements, and also show significant negative Nb-Ti anomalies (Fig. 6b). Interestingly, the trace element features of these three samples match well with those of the Habahe Group terrigenous components as described in Huang et al. (2020a,b) and Jiang et al. (2016).

Granitoid sample 16A10-1 has high SiO₂ (76.40 wt%) and low K₂O (3.82 wt%), TiO₂ (0.10 wt%), Al₂O₃ (12.60 wt%), CaO (0.41 wt%) and MgO (0.38 wt%) contents (Fig. 5b-c, Table 1). It has high-K calc-alkaline and strongly peraluminous composition, with an A/CNK value of 1.35 (Fig. 5e). The sample shows slight enrichment in LREE ([La/Yb]_N = 1.39) and a strongly negative Eu anomaly (Eu/Eu* = 0.42; Fig. 6a). It also shows high contents of LILE (e.g., Ba, Rb, Th and U) and exhibits significant negative anomalies of Nb-Ti on the primitive-normalized spider diagram (Fig. 6b).

Granitoid sample 15AT100-2 has high SiO₂ (67.10 wt%) and low K₂O (1.82 wt%), TiO₂ (0.80 wt%), Al₂O₃ (15.50 wt%), CaO (3.70 wt%) and MgO (1.64 wt%) contents. In the SiO₂ versus Na₂O + K₂O diagram (Cox, 2013), the sample plots into the field of granodiorite (Fig. 5c,

Table 1). In the SiO₂ versus K₂O diagram (Peccerillo and Taylor, 1976), this sample can be classified as calc-alkaline (Fig. 5d). The sample has strong peraluminous signature similar to other samples (A/CNK value of 1.15; Fig. 5e). On the chondrite-normalized REE diagram, this sample displays a weakly positive Eu anomaly (Eu/Eu* = 1.20; Fig. 6a), distinct from the other four samples. The sample shows significantly positive Pb anomaly and enrichment of Rb and Ba with depletion in Nb and Ti on the primitive mantle-normalized multi-elements variation diagram (Fig. 6b).

5.2. Zircon Hf isotopic compositions

Zircons from the metatuff sample 15AT254-1 are 100–150 µm in size and have length/width ratios around 2:1 (Fig. 7a). Most grains show oscillatory zoning in the CL image, suggesting their magmatic origin. Previous U-Pb dating of this type of zircons formed a tight age population corresponding to a weighted mean ²⁰⁶Pb/²³⁸U age of 405.0 ± 1.4 Ma (Broussolle et al., 2018). A few zircons are subhedral

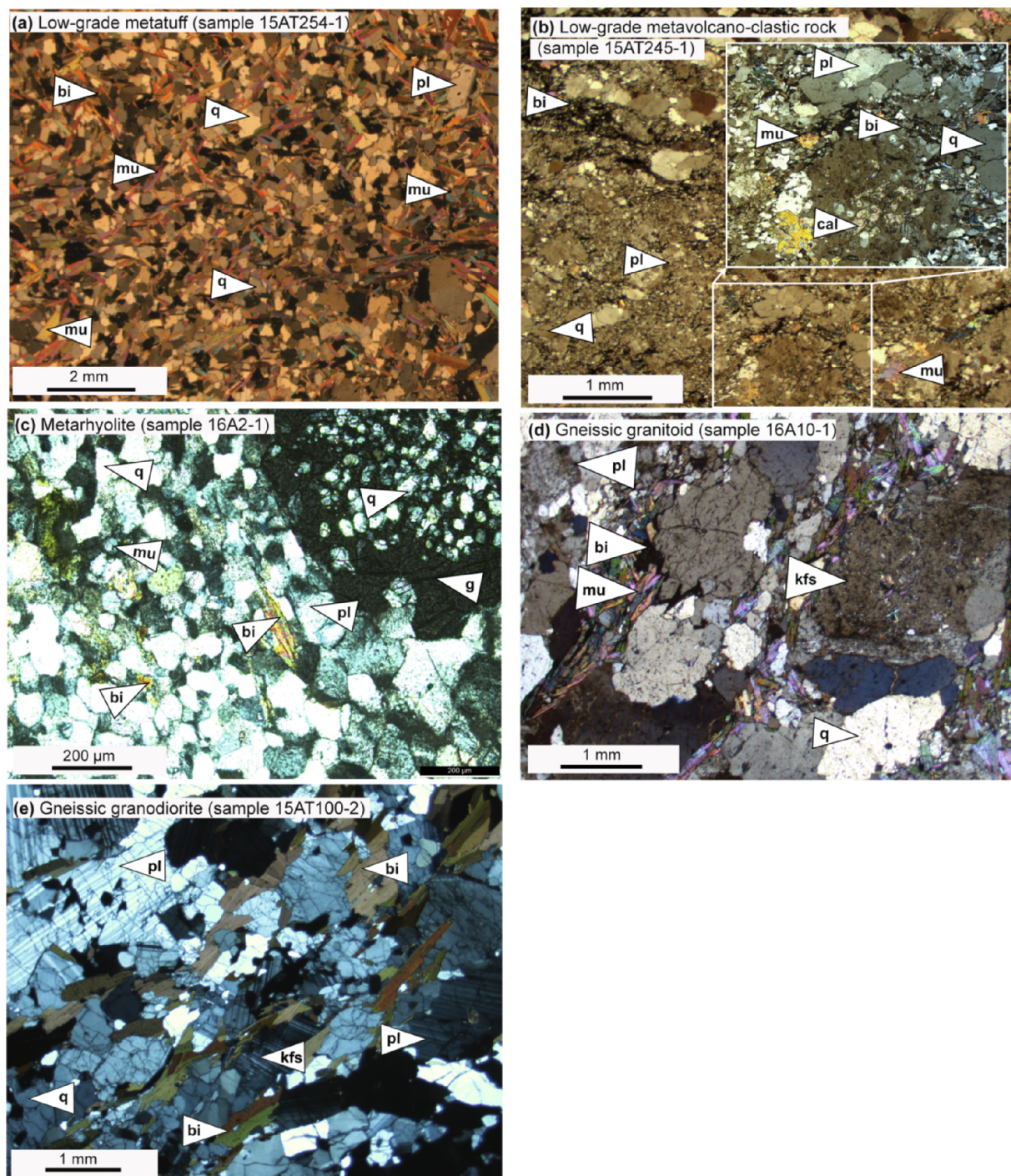


Fig. 4. Microphotographs of magmatic rocks from the Kalasu area. (a) Metatuff, (b) Metavolcano-clastic rock, (c) Metarhyolite, (d) Gneissic granitoid and (e) Gneissic granodiorite.

and some of them have thin metamorphic overgrowths (Fig. 7a). Of these grains some exhibit oscillatory zoning, but others are characterized by very strong or very low luminescence that hardly reveal any internal structures. U-Pb analysis on these grains commonly yielded Middle Cambrian ages (Fig. 7a), interpreted as xenocrysts. Sixteen grains with concordant Devonian ages were selected for Hf isotopic analysis in this study. Fifteen analyses gave $\epsilon_{\text{Hf}}(t)$ values ranging from -2 to $+5$, with T_{DM}^{C} model ages varying from 1.3 to 1.0 Ga. The remaining single grain yielded a very negative $\epsilon_{\text{Hf}}(t)$ value at -26 corresponding to a T_{DM}^{C} model age of ca. 2.7 Ga. Overall, the $\epsilon_{\text{Hf}}(t)$ values are peaking at $+2$, corresponding to a T_{DM}^{C} model age of ca. 1.1 Ga

($n = 15$; Figs. 8a, 9a and Table 2).

Zircons from the metavolcano-clastic sample 15AT245-1 are 100–150 μm in size, stubby, and have length/width ratios mostly ranging from 2:1 to 1:1 (Fig. 7b). All grains are dark grey but still show weak oscillatory zoning, suggesting magmatic origin. Previous U-Pb dating of the sample indicated the majority of zircons formed a tight cluster with a weighted mean $^{206}\text{Pb}/^{238}\text{U}$ age of 395.4 ± 1.7 Ma (Broussolle et al., 2018). Some grains show similar internal structures but gave Ordovician ages, interpreted as xenocrystic zircons (Fig. 7b). Fifteen grains with concordant Devonian ages were selected for Hf isotopic analysis in this study. Fourteen of them yielded mixed $\epsilon_{\text{Hf}}(t)$

Table 2

U-Pb and Hf isotopic analyses of volcanic and granitic rocks from the Kalasu area, SW Altai Orogenic Belt.

Analysis #*	176Hf/177Hf	1 s	176Lu/177Hf	176Yb/177Hf	Age (Ma) **	$\epsilon_{\text{Hf}}^{176\text{Hf}/177\text{Hf}}$	$\epsilon_{\text{Hf}}^{176\text{Hf}/177\text{Hf}}$	\pm (1 s)	TDM (Ma)	\pm (1 s)	TDM ^c (Ma)	\pm (1 s)
Low-grade metatuff (15AT254-1)												
15AT254-1-2	0.282545	0.000017	0.00149	0.03670	404	0.28253	0.44	0.60	1015	24	1204	32
15AT254-1-4	0.282615	0.000015	0.00136	0.03321	397	0.28260	2.81	0.53	912	21	1074	28
15AT254-1-5	0.281822	0.000029	0.00421	0.13501	408	0.28179	-25.80	1.02	2194	44	2569	53
15AT254-1-8	0.282619	0.000012	0.00142	0.03559	403	0.28261	3.08	0.42	907	17	1065	22
15AT254-1-10	0.282539	0.000014	0.00150	0.04189	401	0.28253	0.18	0.47	1023	19	1216	25
15AT254-1-14	0.282654	0.000014	0.00088	0.02202	396	0.28265	4.30	0.47	845	19	995	25
15AT254-1-15	0.282525	0.000015	0.00185	0.04461	403	0.28251	-0.36	0.54	1053	22	1246	28
15AT254-1-16	0.282585	0.000013	0.00124	0.03069	405	0.28258	1.95	0.44	951	18	1126	24
15AT254-1-17	0.282504	0.000015	0.00157	0.03897	405	0.28249	-0.99	0.53	1075	21	1281	28
15AT254-1-18	0.282656	0.000014	0.00078	0.01856	405	0.28265	4.58	0.48	841	19	987	25
15AT254-1-19	0.282635	0.000012	0.00108	0.02685	403	0.28263	3.72	0.41	877	17	1031	22
15AT254-1-20	0.282517	0.000011	0.00162	0.04071	409	0.28250	-0.48	0.40	1059	16	1257	21
15AT254-1-21	0.282469	0.000016	0.00210	0.05242	404	0.28245	-2.39	0.55	1141	23	1353	29
15AT254-1-22	0.282581	0.000012	0.00118	0.02874	403	0.28257	1.79	0.42	955	17	1133	23
15AT254-1-23	0.282619	0.000018	0.00106	0.02586	405	0.28261	3.20	0.64	899	26	1060	34
15AT254-1-25	0.282629	0.000011	0.00108	0.02593	395	0.28262	3.35	0.38	885	15	1044	20
Low-grade metavolcano-clastic (15AT245-1)												
15AT245-1-1	0.282500	0.000012	0.00187	0.04726	394	0.28249	-1.45	0.43	1090	18	1296	23
15AT245-1-2	0.282031	0.000015	0.00490	0.12714	395	0.28199	-18.82	0.51	1917	22	2200	26
15AT245-1-3	0.282613	0.000012	0.00113	0.02774	391	0.28260	2.66	0.42	909	17	1077	22
15AT245-1-4	0.282597	0.000017	0.00133	0.03238	400	0.28259	2.24	0.59	937	24	1107	31
15AT245-1-6	0.282406	0.000017	0.00233	0.05877	398	0.28239	-4.82	0.60	1241	25	1476	31
15AT245-1-7	0.282593	0.000017	0.00137	0.03341	397	0.28258	2.03	0.60	943	24	1115	32
15AT245-1-9	0.282440	0.000010	0.00226	0.05630	388	0.28242	-3.79	0.36	1188	15	1414	19
15AT245-1-13	0.282538	0.000011	0.00145	0.03585	396	0.28253	0.04	0.38	1024	16	1219	20
15AT245-1-22	0.282560	0.000012	0.00147	0.03650	398	0.28255	0.86	0.42	993	17	1177	23
15AT245-1-24	0.282597	0.000012	0.00135	0.03142	398	0.28259	2.20	0.41	937	17	1107	22
15AT245-1-25	0.282521	0.000009	0.00151	0.03724	388	0.28251	-0.75	0.30	1050	12	1254	16
15AT245-1-26	0.282558	0.000012	0.00134	0.03222	402	0.28255	0.91	0.43	992	17	1178	23
15AT245-1-27	0.282518	0.000012	0.00175	0.04348	404	0.28251	-0.56	0.42	1060	17	1257	22
15AT245-1-30	0.282452	0.000016	0.00211	0.05221	398	0.28244	-3.12	0.55	1166	23	1386	29
15AT245-1-35	0.282604	0.000013	0.00137	0.03370	393	0.28259	2.35	0.45	927	18	1095	24
Metarhyolite (16A2-1)												
16A2-1-2	0.282566	0.000016	0.00176	0.04083	391	0.28255	0.86	0.57	992	24	1172	31
16A2-1-4	0.282585	0.000014	0.00189	0.04568	387	0.28257	1.42	0.48	968	20	1139	26
16A2-1-7	0.282468	0.000026	0.00300	0.07137	390	0.28245	-2.94	0.92	1171	39	1371	49
16A2-1-10	0.282612	0.000012	0.00156	0.03615	390	0.28260	2.50	0.42	921	17	1085	23
16A2-1-13	0.282604	0.000013	0.00170	0.03615	391	0.28259	2.22	0.47	935	19	1100	25
16A2-1-17	0.282505	0.000021	0.00265	0.04017	391	0.28249	-1.53	0.75	1106	31	1297	40
16A2-1-19	0.282653	0.000029	0.00085	0.06369	390	0.28265	4.14	1.01	846	41	998	54
16A2-1-26	0.282556	0.000021	0.00193	0.01993	389	0.28254	0.41	0.73	1011	30	1194	39
16A2-1-28	0.282615	0.000020	0.00170	0.03927	389	0.28260	2.57	0.69	919	28	1080	37
16A2-1-31	0.282598	0.000025	0.00149	0.03508	391	0.28259	2.04	0.89	940	36	1110	47
16A2-1-58	0.282435	0.000016	0.00327	0.08087	386	0.28241	-4.26	0.56	1229	24	1436	30
16A2-1-71	0.282420	0.000025	0.00298	0.07179	389	0.28240	-4.67	0.86	1242	36	1460	45
16A2-1-74	0.282287	0.000024	0.00394	0.09730	387	0.28226	-9.66	0.83	1478	36	1719	43
16A2-1-78	0.282501	0.000024	0.00197	0.04760	389	0.28249	-1.53	0.83	1091	34	1296	44
16A2-1-83	0.282555	0.000014	0.00202	0.04833	388	0.28254	0.33	0.49	1015	20	1197	26
Gneissic granitoid (16A10-1)												
16A10-1-3	0.282395	0.000015	0.00254	0.06309	403	0.28238	-5.14	0.52	1263	22	1496	28
16A10-1-4	0.282448	0.000017	0.00163	0.03893	399	0.28244	-3.14	0.61	1158	25	1388	32
16A10-1-6	0.282496	0.000017	0.00197	0.04633	396	0.28248	-1.58	0.58	1099	24	1304	31
16A10-1-8	0.282401	0.000018	0.00203	0.04935	403	0.28239	-4.80	0.63	1237	26	1479	33
16A10-1-20	0.282354	0.000011	0.00276	0.06925	404	0.28233	-6.64	0.39	1331	16	1576	21
16A10-1-26	0.282495	0.000014	0.00184	0.04463	405	0.28248	-1.39	0.50	1096	20	1302	26
16A10-1-27	0.282065	0.000013	0.00498	0.12415	397	0.28203	-17.61	0.46	1869	20	2139	24
16A10-1-50	0.282550	0.000012	0.00136	0.03459	403	0.28254	0.63	0.43	1004	17	1194	23
16A10-1-64	0.282482	0.000014	0.00153	0.03750	403	0.28247	-1.82	0.48	1106	20	1322	26
16A10-1-73	0.282558	0.000017	0.00160	0.03742	401	0.28255	0.82	0.61	999	25	1182	32
16A10-1-74	0.282552	0.000029	0.00092	0.02221	404	0.28255	0.87	1.02	989	41	1182	54
16A10-1-80	0.282328	0.000017	0.00265	0.06666	403	0.28231	-7.57	0.60	1366	25	1623	32
16A10-1-86	0.282301	0.000017	0.00276	0.04207	406	0.28228	-8.50	0.58	1410	24	1674	31
16A10-1-90	0.282461	0.000020	0.00172	0.07020	403	0.28245	-2.61	0.70	1141	28	1364	37
16A10-1-94	0.282571	0.000018	0.00134	0.03237	400	0.28256	1.34	0.63	973	26	1154	34
Gneissic granodiorite (15AT100-2)												
15AT100-2-5	0.282568	0.000012	0.00099	0.02384	411	0.28256	1.55	0.43	969	17	1152	23
15AT100-2-6	0.282592	0.000012	0.00096	0.02262	415	0.28258	2.49	0.40	935	16	1106	21
15AT100-2-10	0.282527	0.000013	0.00140	0.03340	409	0.28252	-0.06	0.44	1038	18	1235	23
15AT100-2-11	0.282536	0.000011	0.00135	0.03212	415	0.28253	0.40	0.39	1024	16	1216	21
15AT100-2-12	0.282522	0.000010	0.00138	0.03487	415	0.28251	-0.09	0.35	1044	14	1242	19
15AT100-2-14	0.282589	0.000014	0.00082	0.02005	416	0.28258	2.43	0.50	936	20	1110	26

(continued on next page)

Table 2 (continued)

Analysis #*	176Hf/177Hf	1 s	176Lu/177Hf	176Yb/177Hf	Age (Ma)**	$(^{176}\text{Hf}/^{177}\text{Hf})_i$	$\epsilon_{\text{Hf}}(t)$	\pm (1 s)	TDM (Ma)	\pm (1 s)	TDM ^c (Ma)	\pm (1 s)
15AT100-2-15	0.282538	0.000012	0.00155	0.03681	416	0.28253	0.45	0.42	1026	17	1214	23
15AT100-2-16	0.282515	0.000011	0.00124	0.03064	414	0.28251	-0.34	0.40	1051	16	1254	21
15AT100-2-20	0.282561	0.000013	0.00125	0.03045	416	0.28255	1.34	0.44	985	18	1167	23
15AT100-2-21	0.282589	0.000010	0.00111	0.02780	408	0.28258	2.18	0.36	943	15	1116	19
15AT100-2-25	0.282462	0.000013	0.00170	0.04266	421	0.28245	-2.17	0.46	1138	19	1355	24
15AT100-2-26	0.282496	0.000013	0.00131	0.03216	415	0.28249	-1.00	0.44	1079	18	1289	24
15AT100-2-27	0.282555	0.000018	0.00118	0.02899	414	0.28255	1.09	0.62	993	25	1179	33
15AT100-2-33	0.282475	0.000012	0.00166	0.04044	413	0.28246	-1.87	0.42	1119	17	1333	22
15AT100-2-34	0.282576	0.000011	0.00108	0.02585	413	0.28257	1.84	0.39	960	16	1138	21

* Analyses numbers correspond to U-Pb dating in Broussolle et al. (2018).

** Ages in Broussolle et al. (2018).

values ranging from -5 to +3 with T_{DM}^{C} model ages varying from 1.5 Ga to 1.1 Ga. Another grain yielded a very negative $\epsilon_{\text{Hf}}(t)$ value of -19, corresponding to a T_{DM}^{C} model age of 2.2 Ga. Collectively, zircons $\epsilon_{\text{Hf}}(t)$ values of the sample cluster around zero corresponding to a T_{DM}^{C} model age of ca. 1.2 Ga (n = 14; Figs. 8b, 9a and Table 2).

Zircons from the metarhyolite sample 16A2-1 are 50–100 μm in size. They are stubby with almost same lengths and widths (Fig. 7c) and most of them show oscillatory zoning, suggesting their magmatic origin. Previous zircon U-Pb dating of the sample yielded a weighted mean $^{206}\text{Pb}/^{238}\text{U}$ age at 388.5 ± 0.9 Ma (Broussolle et al., 2018). Fifteen concordant grains of Devonian age were selected for Hf isotopic analysis in the igneous-related zoned domains, which yielded mixed $\epsilon_{\text{Hf}}(t)$ values ranging from -4.7 to +4.5 with T_{DM}^{C} model age varying from 1.5 to 1.0 Ga. One remaining grain yielded a negative $\epsilon_{\text{Hf}}(t)$ value of -10 corresponding to a T_{DM}^{C} model age of ca. 1.7 Ga. The mean $\epsilon_{\text{Hf}}(t)$ value is about zero corresponding to a T_{DM}^{C} model age peak of ca. 1.2 Ga (n = 14; Figs. 8c, 9a and Table 2).

Zircons from the gneissic granitoid sample 16A10-1 are 100–150 μm in size. They are euhedral to subhedral and show length/width ratios mostly of 3:1 (Fig. 7d). Most grains show oscillatory zoning, suggesting their magmatic origins. Previous zircon U-Pb dating of this type of zircons yielded a weighted mean $^{206}\text{Pb}/^{238}\text{U}$ age of 402.4 ± 1.4 Ma (Broussolle et al., 2018). Besides, few subhedral zircon grains show dark-luminescence cores. These grains yielded Ordovician U-Pb ages interpreted as xenocrystic zircons (Fig. 7d). Fifteen concordant grains with Devonian age were further selected for Hf isotopic analysis. Fourteen grains yielded negative to positive $\epsilon_{\text{Hf}}(t)$ values ranging from -9.0 to +2.0 with T_{DM}^{C} model ages varying from 1.7 Ga to 1.1 Ga. One remaining spot yielded a very negative $\epsilon_{\text{Hf}}(t)$ value of -18 corresponding to a T_{DM}^{C} model age of ca. 2.2 Ga. The mean $\epsilon_{\text{Hf}}(t)$ value of the sample is approximately -3, corresponding to a T_{DM}^{C} model age of ca. 1.4 Ga (n = 14; Figs. 8d, 9a and Table 2).

Zircons from the gneissic granodiorite sample 15AT100-2 are 100–250 μm in size. They are prismatic and show length/width ratios mostly of 3:1 (Fig. 7e). Almost all zircon grains show igneous-related oscillatory zoning. Previous zircon U-Pb dating of the sample yielded a majority of ages between 405 and 420 Ma, with a weighted mean $^{206}\text{Pb}/^{238}\text{U}$ age of 412.2 ± 1.9 Ma (Broussolle et al., 2018). Few grains gave relatively older Cambrian to Ordovician ages, considered as xenocrystic zircons (Fig. 7e). From the analyzed Devonian zircons, fifteen concordant grains were selected for Hf isotopic analysis in this study. These grains yielded $\epsilon_{\text{Hf}}(t)$ values ranging from -2.2 to +2.5 with T_{DM}^{C} model ages varying from ca. 1.4 to 1.1 Ga. The mean $\epsilon_{\text{Hf}}(t)$ value of +0.5 corresponds to a T_{DM}^{C} model age of ca. 1.2 Ga (n = 15; Figs. 8e, 9a and Table 2).

6. Discussion

6.1. Origin and petrogenesis of the igneous rocks

The studied samples show low LOI (loss on ignition) values

(0.33–1.02 wt%), suggesting insignificant chemical alteration (Table 1). This corroborates the fact that no correlations between Rb, Sr, Ba and LOI, which denotes weak to negligible influence of alteration on the chemical compositions. Accordingly, the studied samples generally preserve their primary geochemical and isotopic compositions.

The three felsic volcanic rocks and two granitoids are all strongly peraluminous ($A/\text{CNK} > 1.0$) and most all of them contain muscovite, and less commonly, garnet, as primary minerals (Figs. 4a-e, 5e and 6c), further attesting to their peraluminous composition. Thus, all five studied samples could be considered as typical S-type magmatic rocks similar to the granitoids from the Lachlan orogen (Chappell and Wyborn, 2012; Collins and Richards, 2008; Kemp et al., 2009). It has been documented that strongly peraluminous melts can be generated through hydrous melting of an igneous source or partial melting of a sedimentary source (Chappell and Wyborn, 2012; Jiang et al., 2016; Wolf and Wyllie, 1994). Magma derived from hydrous melting of an igneous source generally have high Sr contents because of preferential breakdown of plagioclase, which will release Al and Sr into the resultant magma (Beard and Lofgren, 1991; Douce, 1996). However, the studied samples all have low Sr and pronounced negative Eu anomalies (Fig. 6a-b, Table 1), suggesting insignificant contribution of plagioclase to the parental magma. Alternatively, our samples show low Rb/Sr, Rb/Ba and $\text{Al}_2\text{O}_3/(\text{MgO} + \text{FeO})$ ratios, compositionally comparable with melts from dehydration melting of an immature sedimentary source, typically the greywacke (Fig. 6d).

It is noteworthy that the Altai wedge sediments, i.e., the Habahe Group, is a greywacke-dominated sequence (e.g., Huang et al., 2020a; Jiang et al., 2016). As pointed out above, the Habahe Group contains a large amount of geochemically immature arc-derived sediments (Huang et al., 2020a; Jiang et al., 2017; Long et al., 2008). Previous studies revealed that the Habahe Group was affected by a prominent Devonian high-temperature metamorphism associated with extensive anatexis in the deep crust (Broussolle et al., 2018). The resulting felsic magmatic rocks formed from the anatexis could share arc-like geochemical signatures reflecting inheritance from the latter source (Figs. 5b and 6e-f), as evidenced by previous thermodynamic and trace element modelling (e.g., Huang et al., 2020a; Jiang et al., 2016; Yu et al., 2019). In other words, the arc-like trace element characteristics of the studied samples only reflect the source rocks rather than the true tectonic environment of their origin. Besides, the varied zircon $\epsilon_{\text{Hf}}(t)$ values (-25 to +5) of the samples are overlapping with those of the Habahe Group (-25 to +15) (Fig. 10a), further attesting the scenario that the felsic magmatic rocks investigated originated from the anatexis of the Habahe Group. In addition, the common presence of Cambrian xenocrystic zircons in the studied rocks also advocates their derivation from the Habahe Group since Cambrian zircons are the dominant population in the Habahe Group (Fig. 7a-e) (Broussolle et al., 2019; Jiang et al., 2011; Long et al., 2007).

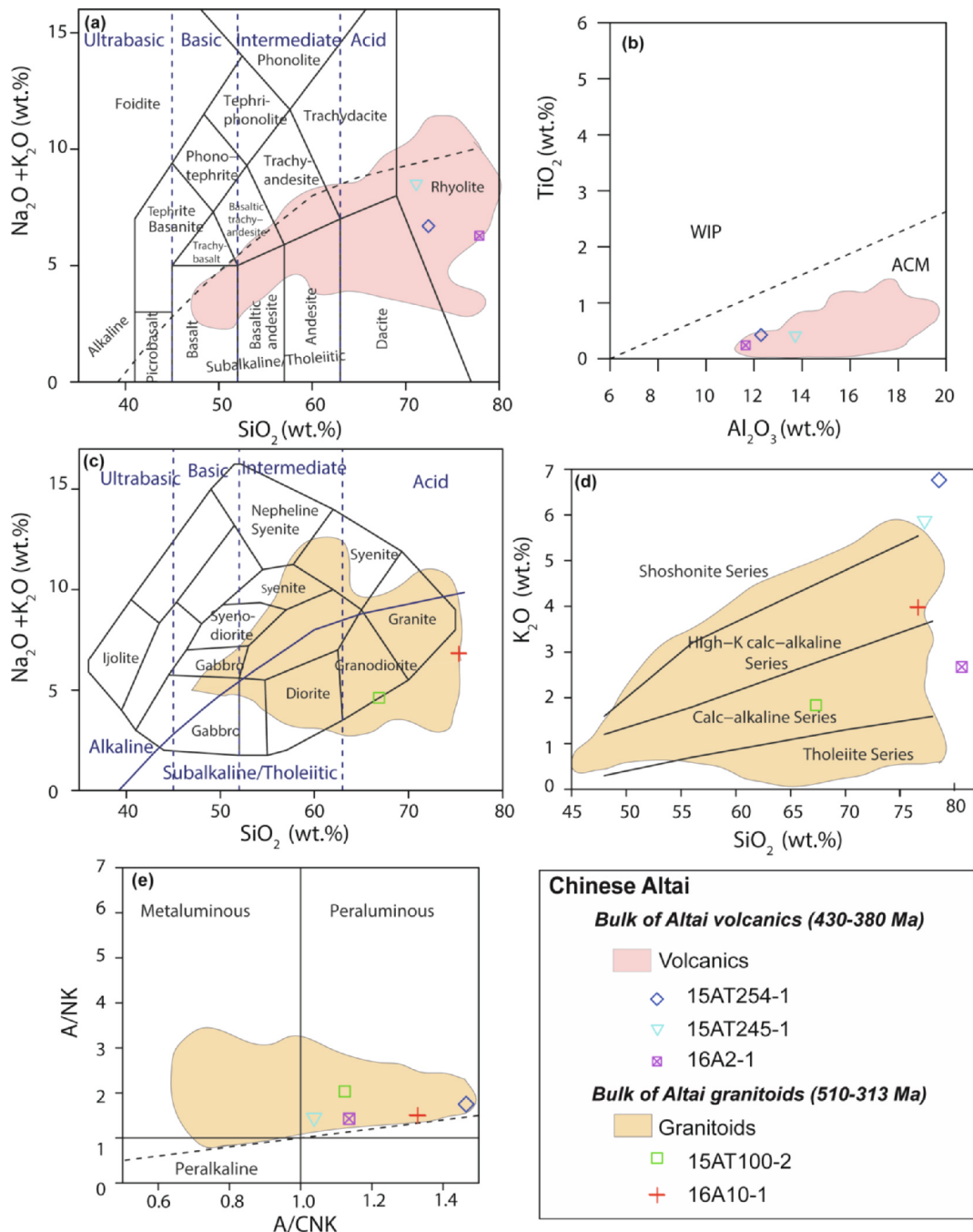


Fig. 5. Geochemical plots for the volcanic rocks and granitoids of the Kalasus area. (a) Total alkalis-silica (TAS) diagram of Le Bas et al. (1986). (b) Geotectonic diagram of Müller et al. (1992). WIP = within plate magmatism and ACM = active continental margin. (c) Total alkalis-silica (TAS) diagram of Cox (2013), (d) SiO_2 vs. K_2O diagram of Peccerillo and Taylor (1976), and (e) A/CNK vs. A/NK diagram of Shand (1943). Data can be found in the Table 1. Data sources for bulk volcanic rocks are from He et al. (2015), Wang et al. (2011), Zhang et al. (2000), and those for bulk granitoids are from Broussolle et al. (2019) and references therein.

6.2. Devonian magmatism in the Chinese Altai: A consequence of lithospheric extension

The Devonian magmatism is the most prevailing magmatic event in the Chinese Altai, as evidenced by the fact that the bulk granitoids in the region have Devonian ages (420–370 Ma, Cai et al., 2011a,b; Wang et al., 2006; Yuan et al., 2007) and occupy more than 40% of the map surface of the Chinese Altai. It has long been noted that these granitoids have calc-alkaline compositions and are enriched in LILE and depleted in HFSE on the N-MORB normalized spider diagrams (Huang et al., 2020a; Jiang et al., 2016). They are also characterized by hybrid crust-mantle geochemistry and variable initial Sr-Nd isotopes (Liu et al., 2012

and references therein). Such geochemical features have led many to suggest that they represent fractionation products of typical continental arc-derived magmas (e.g., Wang et al., 2006; Yuan et al., 2007; Yu et al., 2019). However, this model was based on an assumption that the Chinese Altai was a Precambrian continent block, which is not compatible with recent findings (e.g., Jiang et al., 2011, 2017; Sun et al., 2008). Moreover, to explain the relatively primitive isotopic characteristics of the granitoids, this model also requires input of a large amount of a depleted mantle component (70–90%) in the magma (e.g., Wang et al., 2009a). This is apparently at odds with the facts that mafic enclaves in Devonian granitoids as well as contemporaneous mafic intrusions are relatively rare in the region. It is therefore highly

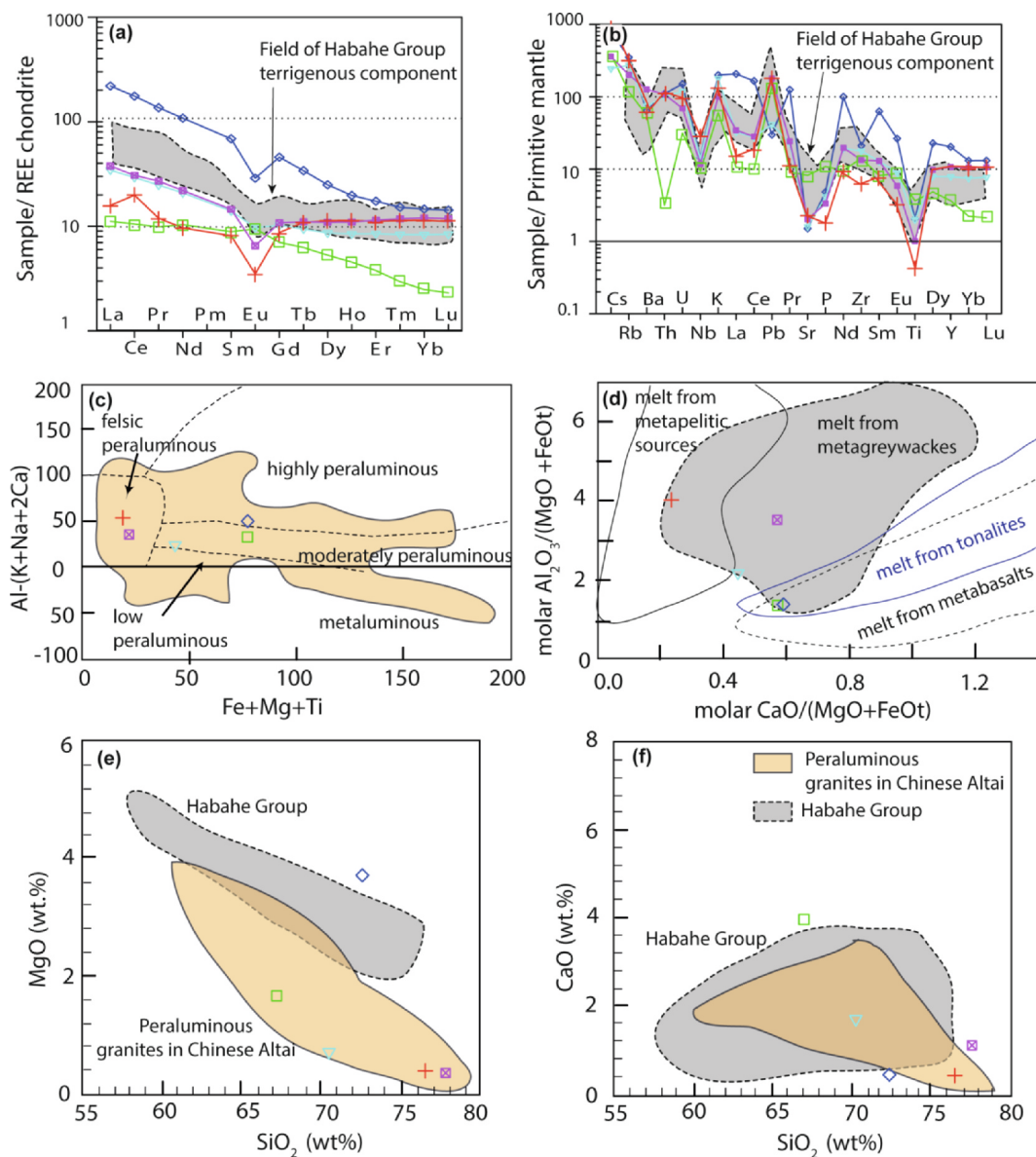


Fig. 6. (a) Chondrite-normalized REE and (b) Primitive mantle normalized trace element patterns for the five magmatic rocks. Chondrite and primitive mantle normalizing values are from Sun and McDonough (1989). The field of Habahe Group metasediments after Huang et al. (2020a) and Jiang et al. (2016) is shown for comparison. (c) ($\text{Fe} + \text{Mg} + \text{Ti}$) vs. $\text{Al} - (\text{K} + \text{Na} + 2\text{Ca})$ diagram of Villaseca et al. (1998) modified from Debon and Le Fort (1983) showing that granitoids from the Kalasu area are characterized by predominantly moderately to highly peraluminous compositions. (d) Binary plot $\text{CaO}/(\text{MgO} + \text{FeO})$ vs. $\text{Al}_2\text{O}_3/(\text{MgO} + \text{FeO})$ (mol %) after Gerdes et al. (2002) to differentiate granitic melts derived from various crustal sources. (e) and (f) are Harker diagrams (SiO_2 vs. MgO and SiO_2 vs. CaO). Legend is the same as previous diagrams. Data are presented in Table 1.

speculative regarding the whole petrogenetic model of the granitoids. Alternatively, a second scenario of magmatic reworking of the Habahe Group has been considered, since the Habahe Group contains abundant young, geochemically immature arc-derived sediments and could serve as a viable source for the granitoids (e.g., Huang et al. 2020a,b; Jiang et al., 2016; Zhang et al. 2017a). It has been suggested that the immature wedge sediments were buried to deep crustal levels as evidenced by the development of a Barrovian-type metamorphic zonation in the metamorphosed wedge with a metamorphic P-max of ~9 kbar (approximately 30 km depth, Burenjargal et al., 2014; Jiang et al., 2015; Wei et al., 2007). This Barrovian metamorphism has been regarded as the response to a progressive convergence during the subduction-accretion evolution of the Chinese Altai in the Early Devonian or earlier (Broussolle et al., 2019; Windley et al., 2002). Later on, the buried sediments were further affected by a high-temperature metamorphism associated with extensive anatexis in the Middle Devonian

(Broussolle et al., 2019; Jiang et al., 2015, 2016). Close temporal and spatial relationship between the anatexis of the Habahe Group rocks and formation/emplacement of the bulk Devonian granitoids has been increasingly found (e.g., Huang et al., 2020a; Jiang et al., 2016, 2019), very similar to that observed in this study (Fig. 3f). Moreover, as cited above, whole-rock geochemistry and pseudosection modelling show that regional anatexis of the Habahe Group could have produced a large amount of melts compositionally similar to the bulk Devonian granitoids in the region (Huang et al., 2020b; Jiang et al., 2016). Recent studies have showed that published whole-rock $\epsilon_{\text{Nd}}(t)$ values of the bulk Devonian granitoids are scattering in a range of -4 to +6 (Wang et al., 2009a and references therein). Such results are falling into the range of the Habahe Group (-7 to +10, Huang et al., 2020b; Jiang et al., 2016 and references therein). The Hf isotopic signatures of the Devonian granitoids can also be attained by mixing of different components of the Habahe Group, as discussed in the following section (Huang et al.,

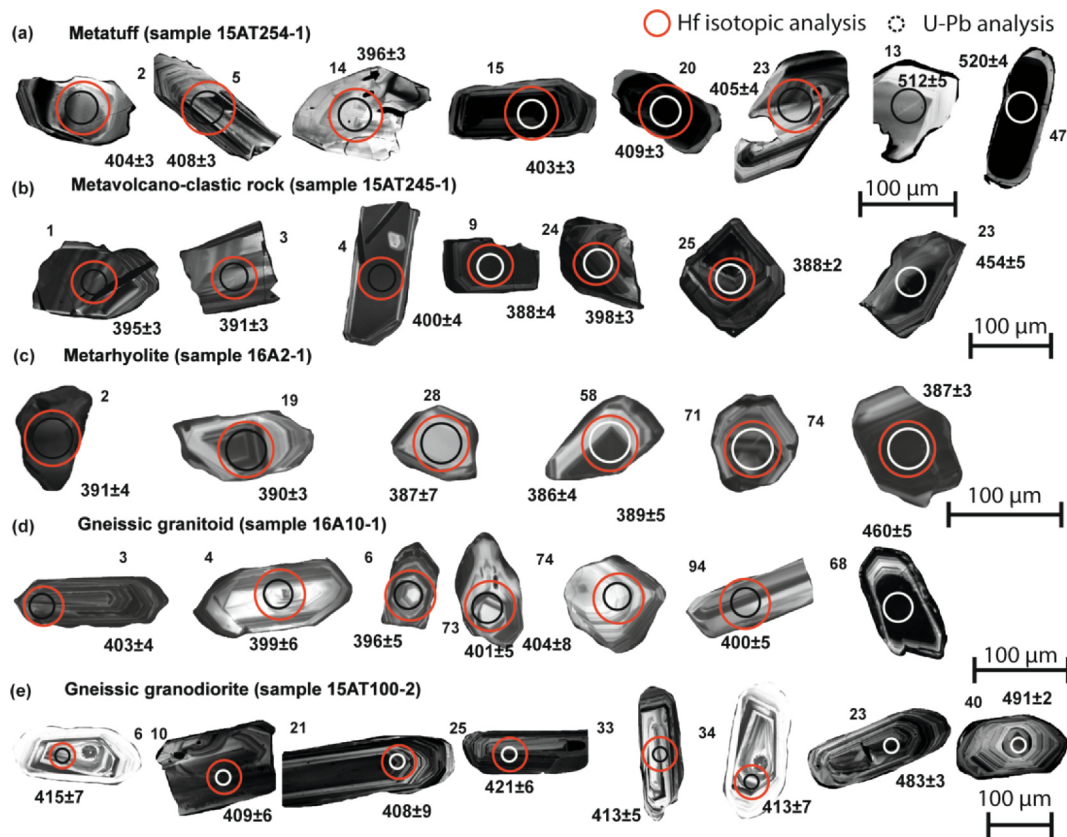


Fig. 7. CL imaging of zircons from the magmatic rocks of the Kalasu area showing the locations of U-Pb and Hf isotopic analyses. U-Pb ages reported in Broussolle et al. (2018) are also indicated.

2020a; Jiang et al., 2016). Based on these data, an updated petrogenetic model for the Altai Devonian granitoids was proposed: the predominant (~85 vol%) peraluminous granitoids (biotite granodiorites to granitoids) could have originated from the greywacke-like Habahe Group while the minor “I-type” hornblende tonalites to granodiorites could either represent magmatic reworking of volcanogenic components of the Habahe Group (e.g., Huang et al., 2020a) or magma mixing between mantle- and crustal-derived components (e.g., Yu et al., 2019). Such a petrogenetic model as well as the compositions of Devonian granitoids in the Chinese Altai match well the classic S-type granites in Circum-Pacific orogens, as exemplified by Collins and Richards (2008).

The anatexis and magmatism cited above is coeval and associated with compositionally heterogeneous mafic rocks and adakite, high-Mg andesite, boninite and Nb-enriched basalt. Such an association was collectively considered as the proxy of an abrupt change in thermal regime due to upwelling of hot asthenospheric mantle (e.g., Ma et al., 2018; Niu et al., 2006; Wong et al., 2010). Subduction of an active spreading oceanic ridge was proposed to explain anomalous thermal conditions of the Chinese Altai in the Devonian (e.g., Ma et al., 2018; Jiang et al., 2010; Sun et al., 2009). However, such a scenario was deduced mainly from geochemical characteristics of magmatic rocks and the details regarding underlying mechanisms as well as spatial-temporal evolution of the ridge subduction have been so far poorly constrained. Alternatively, the elevation of the asthenosphere can be attributed to large-scale lithosphere thinning above the suprasubduction systems, as those documented along the Pacific-type subduction systems (e.g., Collins, 2002; Currie et al., 2004; Hyndman et al., 2005). Jiang et al. (2019) showed that the Devonian tectono-metamorphic evolution of the Chinese Altai is characterized by tectonic switching from shortening to extensional deformation, in association with a metamorphic overprint of a middle-pressure/middle-temperature cycle by a low-pressure/high-temperature one. As a consequence, the deep crust

of the Chinese Altai was affected by horizontal flow of partially molten lower crust dated at about 390 Ma (Broussolle et al., 2019; Jiang et al., 2015; Zhang et al., 2015). At the same time, extrusion of bimodal volcanics occurs in Devonian extensional basins indicate an extensional regime (e.g., Cui et al., 2020; Ma et al., 2018; Soejono et al., 2018; Wan et al., 2011). It should be stressed that polymetallic deposits occur in association with Devonian volcanic rocks and VMS-type Cu-Pb-Zn deposits are representative (Niu et al., 2006). Sulfur and O isotopic studies of ore minerals from some of these deposits imply deep-seated origin of the ore-forming fluids (Niu et al., 2006). Geochemistry of the ore-hosting rocks also showed bi-modal characteristics, advocating the VMS deposits were connected with an extensional environment (Wan et al., 2011). Taken together, the Devonian major thermal event is typical for large heat input from the mantle associated to thinning and horizontal stretching of the whole lithosphere (Broussolle et al., 2018; 2019; Jiang et al., 2016, 2019). We propose that the lithospheric extension therefore accounts for the regional-scale anatexis of the Habahe Group and formation of bulk Devonian granitoids in the region.

6.3. Zircon Hf isotopic features of Devonian granitoids: Towards a better understanding on the nature of the Altai crust

As discussed above, the bulk Devonian granitoids in the Chinese Altai were derived from magmatic reworking of the Habahe Group (Huang et al., 2020a,b; Jiang et al., 2016), and their isotopic signatures could reflect the nature of the deep crust of the Altai wedge. The published whole-rock Nd isotopic signatures of the granitoids support the notion that the origin of bulk Devonian granitoids in the Chinese Altai could be explained by magma mixing in the source between isotopically primitive and evolved components in various proportions (Huang et al., 2020a). However, the bulk Devonian granitoids have so far shown only positive zircon $\epsilon_{\text{Hf}}(t)$ values (0 to +15, Table S1) (e.g.,

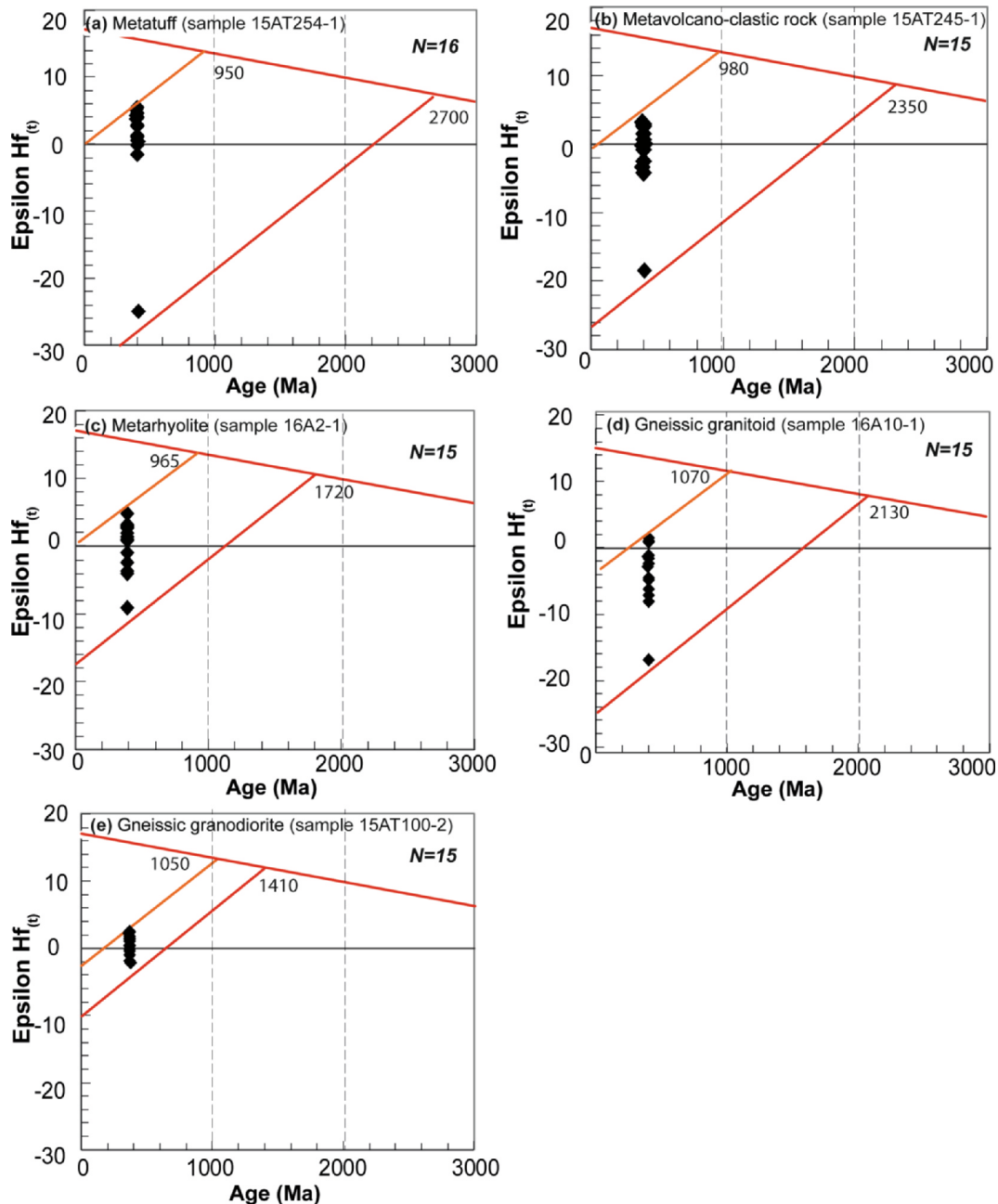


Fig. 8. Zircon $\varepsilon_{\text{Hf}}(t)$ data for the magmatic rocks of the Kalasu area. (a) Metatuff, (b) Metavolcano-clastic rock, (c) Metarhyolite, (d) Gneissic granitoids and (e) Gneissic granodiorite. Data source are listed in Table 2.

Cai et al., 2011a, 2011b, 2012; Dong et al., 2018; Luo et al., 2018; Song et al., 2019; Sun et al., 2008, 2009; Zhang et al., 2017a; Zheng et al., 2016), which are distinctive from those of the Habahe Group that has zircon $\varepsilon_{\text{Hf}}(t)$ values varying from -25 to $+15$ (Fig. 10a, b) (e.g., Jiang et al., 2011; Long et al., 2007, 2010). Thus, unraveling the nature of the deep crust via zircon Hf isotopic signatures of granitoids has so far been elusive.

The studied magmatic rocks are the first report of a significant amount of negative zircon $\varepsilon_{\text{Hf}}(t)$ values in the Chinese Altai (Figs. 8, 9a, Table 2). This may imply that their magma source contains a significant amount of geochemically evolved crustal components. The zircon $\varepsilon_{\text{Hf}}(t)$ values vary from sample to sample, documenting isotopically heterogeneous components in the magma source, i.e., the Habahe Group. For a better understanding of the Altai crust, existing zircon Hf isotopic data for local granitoids were collected for further discussion (Table S1). Instead of presenting single zircon Hf data, an average $\varepsilon_{\text{Hf}}(t)$ value was

calculated for each investigated rock (Fig. 11 and Table S1). The spatial and temporal distribution of mean $\varepsilon_{\text{Hf}}(t)$ values are further portrayed on a map of the region (Fig. 11).

It is shown that zircon Hf isotopic data of the bulk Devonian granitoids varied from -4 to $+18$, and can be broadly subdivided into 5 groups: -3.8 to -1.2 , -1.2 to $+1.2$, $+1.2$ to $+5$, $+5$ to $+8.5$ and $+8.5$ to $+14.5$, irrespective to the formation ages of the granitoids (Fig. 11). The random Hf isotopic values traversing the Chinese Altai from north to south advocates that the region is composed of diverse components (Broussolle et al., 2019; Huang et al., 2020a; Jiang et al., 2019), rather than a series of southward younging terranes (Song et al., 2019; Wang et al., 2009a; Windley et al., 2002; Zhang et al. 2017b). In fact, the detailed granitoids Nd-Sr isotopic mapping of Wang et al. (2009a) exhibited dissimilar characteristics between the southern Chinese Altai and the remaining part of the Chinese Altai (see the Fig. 5 in Wang et al., 2009a). However, the major part of the Chinese Altai has a

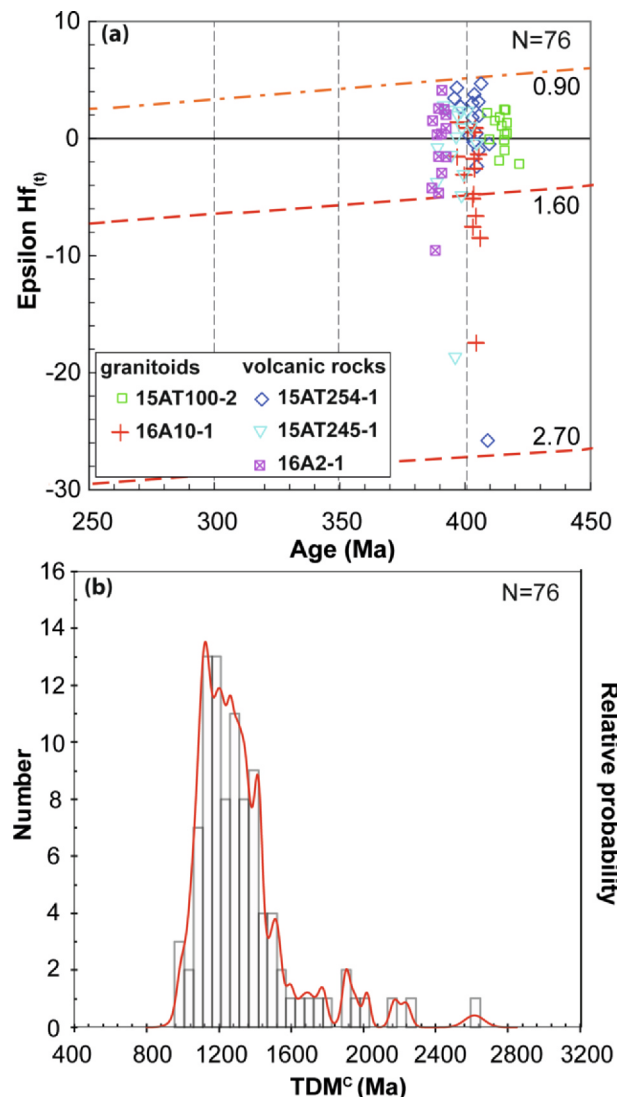


Fig. 9. (a) Zircon Hf isotopic features for the five studied magmatic rocks in the Kalasu area. (b) Probability density plot for T_{DM}^c model ages for the five studied magmatic rocks. See Table 2 for data source.

quite homogenous Nd isotopic signature, which do not support a general southward depleted trend as has been claimed (e.g., Song et al., 2019; Wang et al., 2009a; Zhang et al. 2017b). Nevertheless, the variable $\epsilon_{Hf}(t)$ signatures are overlapping with those of the Habahe Group (Fig. 10a, b), further attesting magmatic reworking of the Ordovician wedge sediments, i.e., the Habahe Group. The bulk $\epsilon_{Hf}(t)$ values are mainly positive, attesting that the region contains abundant chemically juvenile components as proposed in previous studies (e.g., Cai et al., 2011a, 2011b, 2012; Dong et al., 2018; He et al., 2018; Huang et al., 2020; Jiang et al., 2016; Song et al., 2019; Sun et al., 2008, 2009).

Even if there is no general isotopic trend from the north to south, the Hf isotopic data for the local granitoids show broadly dissimilar features in the three different domains, regardless of each domain also shows notable variations of $\epsilon_{Hf}(t)$ values. The northwest domain is characterized by almost all positive mean $\epsilon_{Hf}(t)$ values varying from +1.2 to +14.5, the central domain near the studied area has most enriched $\epsilon_{Hf}(t)$ values mainly ranging from -3.8 to +5, and the southeast domain has $\epsilon_{Hf}(t)$ values broadly falling in between the former two domains (Fig. 11). The positive $\epsilon_{Hf}(t)$ values may suggest significant juvenile components present in the magma source while the negative values imply the contribution of evolved ancient crustal components. Those ancient crustal components can be interpreted as

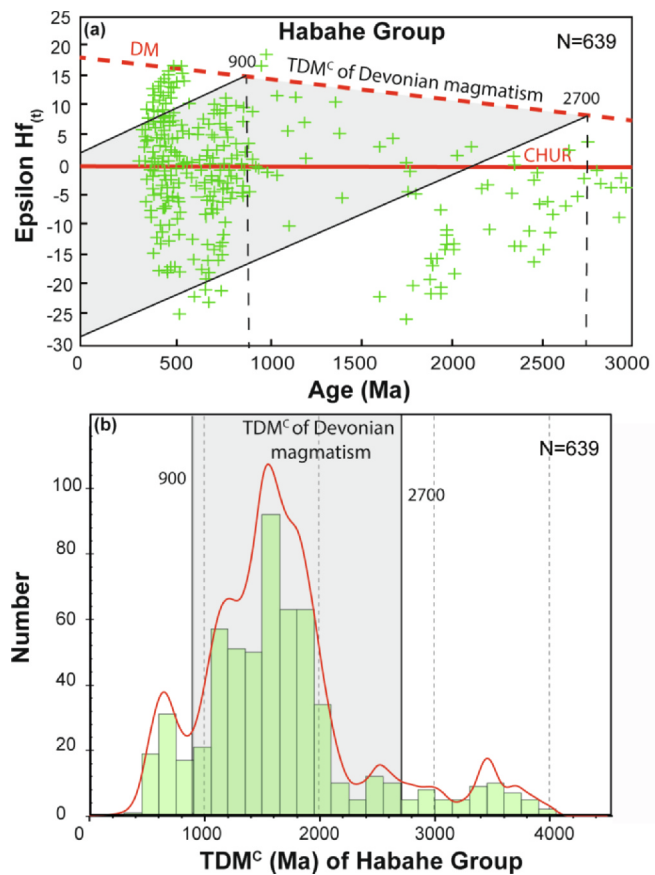


Fig. 10. (a) Diagram of zircon $\epsilon_{Hf}(t)$ values versus ages for the Habahe Group rocks. (b) Probability density plot for T_{DM}^c model ages for the Habahe Group rocks. The field for the Devonian granitoids from this study is indicated. Data source for the Habahe Group rocks can be found in Broussolle et al. (2019 and references therein).

detritus derived from the Tuva-Mongol continental ribbons further north as discussed in previous studies (Broussolle et al., 2019; Jiang et al., 2011; Long et al., 2007, 2008). Apparently, magmatic reworking in the study area has imaged more contribution of ancient crustal components compared with the other two domains. All together, these features suggest that the nature of the deep crust imaged by zircon Hf isotopic signatures is literally heterogeneous. In other words, the results from this work further attest that the Altai prism received both chemically juvenile and more evolved ancient crustal components in general (e.g., Huang et al., 2020b; Jiang et al., 2016, 2017; Zhang et al., 2017a).

7. Conclusions

1. Felsic magmatic rocks in the Kalasu area are characterized by peraluminous compositions and show similar trace element patterns with the Ordovician wedge sediments, i.e., the Habahe Group. Our data show that these Devonian magmatic rocks originated from magmatic reworking of the Altai accretionary wedge (i.e., S-type magmatism).
2. Zircon Hf isotopic data of these felsic magmatic rocks yielded a significant amount of negative $\epsilon_{Hf}(t)$ values, the first time for the region, documenting the reworking of isotopically much evolved ancient crustal components in the magma source.
3. The Devonian magmatism associated with extensive anatexic reworking of the pre-existing Ordovician wedge sediments was probably connected with an important lithospheric extension in the Chinese Altai.

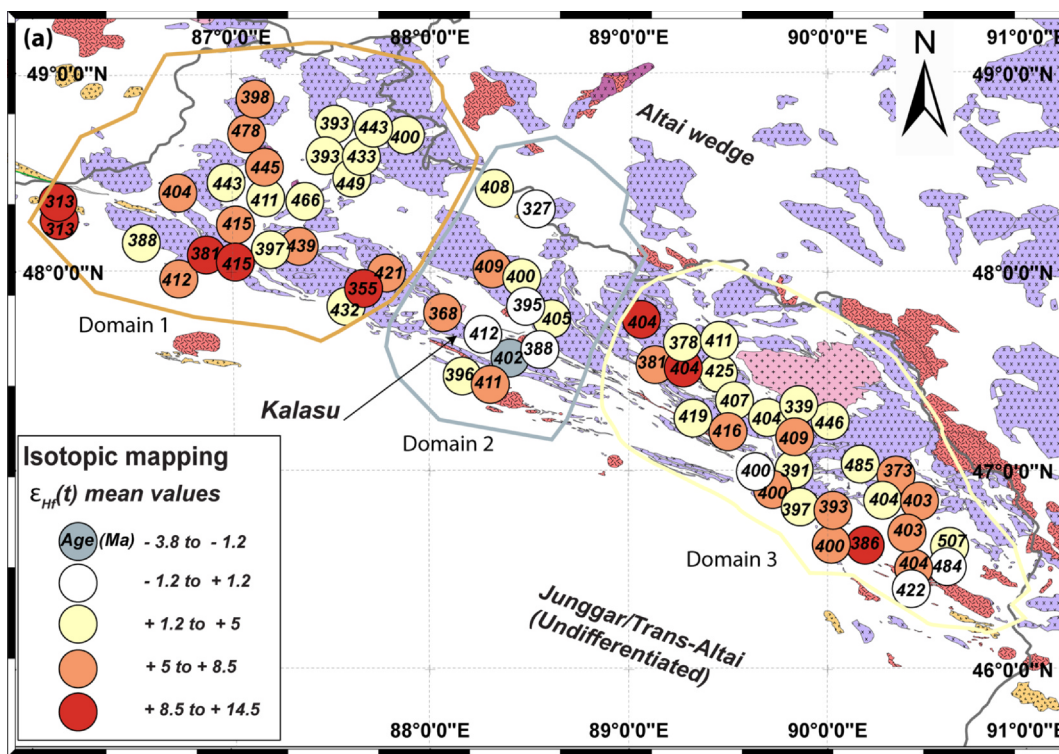


Fig. 11. Plot of regional existing zircon $\epsilon_{\text{Hf}}(t)$ values of magmatic rocks from the Chinese Altai. Three domains with dissimilar ranges of $\epsilon_{\text{Hf}}(t)$ values can be identified. The $\epsilon_{\text{Hf}}(t)$ isotopic values of each granitoid investigated are calculated as mean values (see text for further explanation, Table S1). Hf-in-zircon data were collected from the following sources (Cai et al., 2011a, 2011b, 2012; Dong et al., 2018; He et al., 2018; He et al., 2015; Luo et al., 2018; Ma, 2014; Song et al., 2017; Song et al., 2019; Sun et al., 2008, 2009; Wang et al., 2011; Zhang et al., 2017a; Zheng et al., 2016). Legend is the same as Fig. 1.

4. Mapping of $\epsilon_{\text{Hf}}(t)$ values for the bulk Devonian granitoids in the Chinese Altai displays three isotopically dissimilar domains, suggesting the perspective that the Ordovician Altai wedge, i.e., the Habahe Group, in the deep crust, is compositionally heterogeneous.

Credit author statement

Conceptualization: Arnaud Broussolle and Yingde Jiang. Data curation: Arnaud Broussolle. Funding acquisition: Min Sun, Yingde Jiang, Tan Shu, Arnaud Broussolle. Writing - original draft: Arnaud Broussolle, Yingde Jiang, Yang Yu and Min Sun. Writing - review and editing: Arnaud Broussolle, Yingde Jiang, Min Sun, Yang Yu and Jean Wong. Data acquisition: Arnaud Broussolle, Kang Xu, Tan Shu and Jean Wong.

Declaration of Competing Interest

The authors declare that they have no known competing financial interests or personal relationships that could have appeared to influence the work reported in this paper.

Acknowledgements

Miss Xiao Fu is thanked for helping for sample preparation and processing whole-rock data at the Department of Earth Sciences, The University of Hong Kong, China. This study was supported by the International Partnership Program of Chinese Academy of Sciences (132744KYSB20190039), NSF China (41672056), the National Key R&D Program of China (Grant No. 2017YFC0601205) and Hong Kong RGC grants (17303415 and 17302317). A International Postdoctoral Exchange Fellowship Program (Talent-Introduction Program) and a Foundation of Director of Guangzhou Institute of Geochemistry, Chinese Academy of Sciences (2019SZJJ-11) to Dr. A. Broussolle and a

Guangdong Special Support Program to Y.D. Jiang are also acknowledged. This is contribution No. IS-2906 from GIGCAS and also a contribution to IGCP 662. Dr. Carmen Aguilar is thanked for polishing figure 1 and 2 and contributing to figure 4 that Arnaud modified from the previous publication. Dr. Stephen Collett is thanked for reading the manuscript. We thank one anonymous reviewer and Dr. Shan Li for their constructive comments that have greatly improved the manuscript.

Appendix A. Supplementary material

Supplementary data to this article can be found online at <https://doi.org/10.1016/j.jseaes.2020.104538>.

References

- Augustsson, C., Willner, A.P., Rüsing, T., Niemeyer, H., Gerdes, A., Adams, C.J., Miller, H., 2016. The crustal evolution of South America from a zircon Hf-isotope perspective. *Terra Nova* 28 (2), 128–137.
- Beard, J.S., Lofgren, G.E., 1991. Dehydration melting and water saturated melting of basaltic and andesitic greenstones and amphibolites at 1, 3, and 7 kb. *J. Petrol.* 32, 365–401.
- BGMRX, 1978. Geological Map of the Altai Sheet: Scale1: 200,000 (Unpublished).
- Blichert-Toft, J., Albarède, F., 1997. The Lu-Hf isotope geochemistry of chondrites and the evolution of the mantle-crust system. *Earth Planet. Sci. Lett.* 148 (1–2), 243–258.
- Burenjargal, U., Okamoto, A., Kuwatani, T., Sakata, S., Hirata, T., Tsuchiya, N., 2014. Thermal evolution of the Tseel terrane, SW Mongolia and its relation to granitoid intrusions in the Central Asian Orogenic Belt. *J. Metamorph. Geol.* 32 (7), 765–790.
- Broussolle, A., Aguilar, C., Sun, M., Schulmann, K., Štípká, P., Jiang, Y., Yu, Y., Xiao, W., Wang, S., Miková, J., 2018. Polycyclic Palaeozoic evolution of accretionary orogenic wedge in the southern Chinese Altai: evidence from structural relationships and U-Pb geochronology. *Lithos* 314–315, 400–424.
- Broussolle, A., Sun, M., Schulmann, K., Guy, A., Aguilar, C., Štípká, P., Jiang, Y., Yu, Y., Xiao, W., 2019. Are the Chinese Altai “terranes” the result of juxtaposition of different crustal levels during Late Devonian and Permian orogenesis? *Gondwana Res.* 66, 183–206.
- Cai, K., Sun, M., Yuan, C., Xiao, W., Zhao, G., Long, X., Wu, F., 2012. Carboniferous mantle-derived felsic intrusion in the Chinese Altai, NW China: Implications for geodynamic change of the accretionary orogenic belt. *Gondwana Res.* 22 (2), 681–698.

- Cai, K., Sun, M., Yuan, C., Zhao, G., Xiao, W., Long, X., Wu, F., 2011a. Geochronology, petrogenesis and tectonic significance of peraluminous granites from the Chinese Altai, NW China. *Lithos* 127 (1), 261–281.
- Cai, K., Sun, M., Yuan, C., Zhao, G., Xiao, W., Long, X., Wu, F., 2011b. Prolonged magmatism, juvenile nature and tectonic evolution of the Chinese Altai, NW China: evidence from zircon U-Pb and Hf isotopic study of Paleozoic granitoids. *J. Asian Earth Sci.* 42 (5), 949–968.
- Cawood, P.A., Buchan, C., 2007. Linking accretionary orogenesis with supercontinent assembly. *Earth Sci. Rev.* 82 (3), 217–256.
- Cawood, P.A., Kröner, A., Collins, W.J., Kusky, T.M., Mooney, W.D., Windley, B.F., 2009. Accretionary orogens through Earth history. *Geol. Soc. Lond. Special Publ.* 318, 1–36.
- Chai, F.M., Mao, J.W., Dong, L.H., Yang, F.Q., Liu, F., Geng, X.X., Zhang, Z.X., 2009. Geochronology of metarhyolites from the Kangbutiebao Formation in the Kelang basin, Altay Mountains, Xinjiang: implications for the tectonic evolution and metallogeny. *Gondwana Res.* 16, 189–200.
- Chappell, B.W., Wyborn, D., 2012. Origin of enclaves in S-type granites of the Lachlan Fold Belt. *Lithos* 154, 235–247.
- Chen, B., Jahn, B.M., 2002. Geochemical and isotopic studies of the sedimentary and granitic rocks of the Altai orogen of northwest China and their tectonic implications. *Geol. Mag.* 139 (1), 1–13.
- Chen, M., Sun, M., Cai, K., Buslov, M.M., Zhao, G., Rubanova, E.S., Voytishev, E.E., 2014. Detrital zircon record of the early Paleozoic meta-sedimentary rocks in Russian Altai: Implications on their provenance and the tectonic nature of the Altai-Mongolian terrane. *Lithos* 233, 209–222.
- Collins, W.J., 2002. Hot orogens, tectonic switching, and creation of continental crust. *Geology* 30 (6), 535–538.
- Collins, W., Richards, S., 2008. Geodynamic significance of S-type granites in circum-Pacific orogens. *Geology* 36 (7), 559–562.
- Cox, K.G.E., 2013. The Interpretation of Igneous Rocks. Springer Science & Business Media.
- Cui, X., Sun, M., Zhao, G., Yao, J., Zhang, Y., Han, Y., Dai, L., 2020. A Devonian arc-back-arc basin system in the southern Chinese Altai: Constraints from geochemical and Sr-Nd-Pb isotopic data for meta-basaltic rocks. *Lithos*. <https://doi.org/10.1016/j.lithos.2020.105540>.
- Currie, C.A., Wang, K., Hyndman, R.D., He, J., 2004. The thermal effects of steady-state slab-driven mantle flow above a subducting plate: The Cascadia subduction zone and backarc. *Earth Planet. Sci. Lett.* 223 (1–2), 35–48.
- Debon, F., Le Fort, P., 1983. A chemical-mineralogical classification of common plutonic rocks and associations. *Earth Environ. Sci. Trans. R. Soc. Edinburgh* 73 (3), 135–149.
- Dong, Z., Han, Y., Zhao, G., Pan, F., Wang, K., Huang, B., Chen, J., 2018. Zircon U-Pb ages and Hf isotopes of Paleozoic metasedimentary rocks from the Habae Group in the Qinghe area, Chinese Altai and their tectonic implications. *Gondwana Res.* 61, 100–114.
- Douce, A., 1996. Effects of pressure and H₂O content on the compositions of primary crustal melts. *Earth Environ. Sci. Trans. R. Soc. Edinburgh* 87 (1–2), 11–21.
- Gerdes, A., Montero, P., Bea, F., Ferschater, G., Borodina, N., Osipova, T., Shardakova, G., 2002. Peraluminous granites frequently with mantelike isotope compositions: The continental-type Murzinka and Dzhabyk batholiths of the eastern Urals. *Int. J. Earth Sci.* 91 (1), 3–19.
- Gray, D.R., Foster, D.A., 2004. Tectonic evolution of the Lachlan Orogen, southeast Australia: historical review, data synthesis and modern perspectives. *Aust. J. Earth Sci.* 51 (6), 773–817.
- Griffin, W.L., Pearson, N.J., Belousova, E., Jackson, S.E., van Achterbergh, E., O'Reilly, S.Y., Shee, S.R., 2000. The Hf isotope composition of cratonic mantle: LAM-MC-ICPMS analysis of zircon megacrysts in kimberlites. *Geochim. Cosmochim. Acta* 64 (1), 133–147.
- Griffin, W.L., Wang, X., Jackson, S.E., Pearson, N.J., O'Reilly, S.Y., Xu, X., Zhou, X., 2002. Zircon chemistry and magma mixing, SE China: In-situ analysis of Hf isotopes, Tonglu and Pingtan igneous complexes. *Lithos* 61 (3–4), 237–269.
- Guy, A., Schulmann, K., Soejono, I., Xiao, W., 2020. Revision of the Chinese Altai - East Junggar terrane accretion model based on geophysical and geological constraints. *Tectonics* 39 (4). <https://doi.org/10.1029/2019TC006026>.
- He, D., Dong, Y., Xu, X., Chen, J., Liu, X., Li, W., Li, X., 2018. Geochemistry, geochronology and Hf isotope of granitoids in the Chinese Altai: Implications for Paleozoic tectonic evolution of the Central Asian Orogenic Belt. *Geosci. Front.* 9 (5), 1399–1415.
- He, Y., Sun, M., Cai, K., Xiao, W., Zhao, G., Long, X., Li, P., 2015. Petrogenesis of the Devonian high-Mg rock association and its tectonic implication for the Chinese Altai orogenic belt, NW China. *J. Asian Earth Sci.* 113, 61–74.
- Hu, A., Jahn, B.-M., Zhang, G., Chen, Y., Zhang, Q., 2000. Crustal evolution and Phanerozoic crustal growth in northern Xinjiang: Nd isotopic evidence. Part I. Isotopic characterization of basement rocks. *Tectonophysics* 328 (1), 15–51.
- Huang, Y., Jiang, Y., Collett, S., Wang, S., Xu, K., Shu, T., Li, P., Yuan, C., 2020a. Magmatic recycling of accretionary wedge: A new perspective on Silurian-Devonian I-type granitoids generation in the Chinese Altai. *Gondwana Res.* 78, 291–307.
- Huang, Y., Jiang, Y., Yu, Y., Collett, S., Wang, S., Shu, T., Xu, K., 2020b. Nd-Hf Isotopic Decoupling of the Silurian–Devonian Granitoids in the Chinese Altai: A Consequence of Crustal Recycling of the Ordovician Accretionary Wedge? *J. Earth Sci.* 31, 102–114.
- Hyndman, R.D., Currie, C.A., Mazzotti, S., 2005. Subduction zone backarcs, continental mobile belts, and orogenic heat. *Geol. Soc. Am. Today* 15, 4–10.
- Jahn, B.M., Wu, F., Chen, B., 2000. Granitoids of the Central Asian Orogenic Belt and continental growth in the Phanerozoic. *Trans. R. Soc. Edinburgh Earth Sci.* 91 (1–2), 181.
- Janoušek, V., Farrow, C.M., Erban, V., 2006. Interpretation of whole-rock geochemical data in igneous geochemistry: introducing Geochemical Data Toolkit (GCDkit). *J. Petrol.* 47 (6), 1255–1259.
- Janoušek, V., Jiang, Y., Buriánek, D., Schulmann, K., Hanžl, P., Soejono, I., Kröner, A., Altanbaatar, B., Erban, V., Lexa, O., Ganchuluun, T., Košler, J., 2018. Cambrian-Ordovician magmatism of the Ikh-Mongol Arc System exemplified by the Khantaishir Magmatic Complex (Lake Zone, south-central Mongolia). *Gondwana Res.* 54, 122–149.
- Jiang, Y.D., Schulmann, K., Sun, M., Štípká, P., Guy, A., Janoušek, V., Lexa, O., Yuan, C., 2016. Anatexis of accretionary wedge, Pacific-type magmatism, and formation of vertically stratified continental crust in the Altai Orogenic Belt. *Tectonics* 35, 3095–3118.
- Jiang, Y.D., Schulmann, K., Kröner, A., Sun, M., Lexa, O., Janoušek, V., Buriánek, D., Yuan, C., Hanžl, P., 2017. Neoproterozoic-early paleozoic peri-pacific accretionary evolution of the mongolian collage system: insights from geochemical and U-Pb zircon data from the ordovician sedimentary wedge in the Mongolian Altai. *Tectonics* 36 (11), 2305–2331.
- Jiang, Y.D., Schulmann, K., Sun, M., Weinberg, R.F., Štípká, P., Li, P.F., Zhang, J., Chopin, F., Wang, S., Xia, X.P., Xiao, W.J., 2019. Structural and geochronological constraints on Devonian suprasubduction tectonic switching and Permian collisional dynamics in the Chinese Altai. *Central Asia. Tectonics* 38 (1), 253–280.
- Jiang, Y.D., Štípká, P., Sun, M., Schulmann, K., Zhang, J., Wu, Q.H., Long, X.P., Yuan, C., Racek, M., Zhao, G.C., Xiao, W.J., 2015. Juxtaposition of Barrovian and migmatitic domains in the Chinese Altai: a result of crustal thickening followed by doming of partially molten lower crust. *J. Metamorph. Geol.* 33 (1), 45–70.
- Jiang, Y.D., Sun, M., Zhao, G., Yuan, C., Xiao, W., Xia, X., Wu, F., 2011. Precambrian detrital zircons in the Early Paleozoic Chinese Altai: their provenance and implications for the crustal growth of central Asia. *Precambr. Res.* 189 (1), 140–154.
- Jiang, Y.D., Sun, M., Zhao, G.C., Yuan, C., Xiao, W., Xia, X.P., Long, X.P., Wu, F.Y., 2010. The ~390 Ma high-T metamorphic event in the Chinese Altai: A consequence of ridge-subduction? *Am. J. Sci.* 310 (10), 1421–1452.
- Kemp, A., Hawkesworth, C., Collins, W., Gray, C., Blevin, P., 2009. Isotopic evidence for rapid continental growth in an extensional accretionary orogen: The Tasmanides, eastern Australia. *Earth Planet. Sci. Lett.* 284 (3), 455–466.
- Kröner, A., Kovach, V., Belousova, E., Hegner, E., Armstrong, R., Dolgopolova, A., Seltmann, R., Alexeev, D.V., Hoffmann, J.E., Wong, J., Sun, M., Cai, K., Wang, T., Tong, Y., Wilde, S.A., Degtyarev, K.E., Rytsk, E., 2014. Reassessment of continental growth during the accretionary history of the Central Asian Orogenic Belt. *Gondwana Res.* 25 (1), 103–125.
- Kusky, T.M., Windley, B.F., Safonova, I., Wakita, K., Wakabayashi, J., Polat, A., Santosh, M., 2013. Recognition of ocean plate stratigraphy in accretionary orogens through Earth history: A record of 3.8 billion years of sea floor spreading, subduction, and accretion. *Gondwana Res.* 24 (2), 501–547.
- Le Bas, M.J., Le Maitre, R.W., Streckeisen, A., Zanettin, B., 1986. A chemical classification of volcanic rocks based on the total alkali-silica diagram. *J. Petrol.* 27, 745–750.
- Li, P., Sun, M., Rosenbaum, G., Jourdan, F., Li, S., Cai, K., 2017. Late Paleozoic closure of the Ob-Zaisan Ocean along the Irtysh shear zone (NW China): Implications for arc amalgamation and ooclinal bending in the Central Asian orogenic belt. *Geol. Soc. Am. Bull.* 129 (5–6), 547.
- Li, P., Sun, M., Shu, C., Yuan, C., Jiang, Y., Zhang, L., Cai, K., 2019. Evolution of the Central Asian Orogenic Belt along the Siberian margin from Neoproterozoic-Early Paleozoic accretion to Devonian trench retreat and a comparison with Phanerozoic eastern Australia. *Earth Sci. Rev.* 198, 102–121.
- Li, X.-H., Li, Z.-X., Wingate, M.T.D., Chung, S.-L., Liu, Y., Lin, G.-C., Li, W.-X., 2006. Geochemistry of the 755Ma Mundine Well dyke swarm, northwestern Australia: Part of a Neoproterozoic mantle superplume beneath Rodinia? *Precambr. Res.* 146 (1), 1–15.
- Li, Z., Yang, X., Li, Y., Santosh, M., Chen, H., Xiao, W., 2014. Late Paleozoic tectono-metamorphic evolution of the Altai segment of the Central Asian Orogenic Belt: Constraints from metamorphic P-T pseudosection and zircon U-Pb dating of ultra-high-temperature granulite. *Lithos* 204, 83–96.
- Lin, Z., Yuan, C., Zhang, Y., Sun, M., Long, X., Wang, X., Huang, Z., Chen, Z., 2019. Petrogenesis and geodynamic implications of two episodes of Permian and Triassic high-silica granitoids in the Chinese Altai, Central Asian Orogenic Belt. *J. Asian Earth Sci.* 184, 103978.
- Liu, W., Liu, X.J., Xiao, W.J., 2012. Massive granitoid production without massive continental-crust growth in the Chinese Altay: Insight into the source rock of granitoids using integrated zircon U-Pb age, Hf-Nd-Sr isotopes and geochemistry. *Am. J. Sci.* 312 (6), 629–684.
- Liu, Y., Zhang, H., Tang, Y., Zhang, X., Lv, Z., Zhao, J., 2018. Petrogenesis and tectonic setting of the Middle Permian A-type granites in Altay, northwestern China: Evidences from geochronological, geochemical, and Hf isotopic studies. *Geol. J.* 53 (2), 527–546.
- Liu, Z., Bartoli, O., Tong, L., Xu, Y.G., Huang, X., 2020. Permian ultrahigh-temperature reworking in the southern Chinese Altai: Evidence from petrology, P-T estimates, zircon and monazite U-Th-Pb geochronology. *Gondwana Res.* 78, 20–40.
- Long, X., Sun, M., Yuan, C., Xiao, W., Cai, K., 2008. Early Paleozoic sedimentary record of the Chinese Altai: Implications for its tectonic evolution. *Sed. Geol.* 208 (3–4), 88–100.
- Long, X., Sun, M., Yuan, C., Xiao, W., Lin, S., Wu, F., Cai, K., 2007. Detrital zircon age and Hf isotopic studies for metasedimentary rocks from the Chinese Altai: Implications for the Early Paleozoic tectonic evolution of the Central Asian Orogenic Belt. *Tectonics* 26 (5), 1–20.
- Long, X., Yuan, C., Sun, M., Xiao, W., Wang, Y., Cai, K., Jiang, Y., 2012. Geochemistry and Nd isotopic composition of the Early Paleozoic flysch sequence in the Chinese Altai, Central Asia: Evidence for a northward-derived mafic source and insight into Nd model ages in accretionary orogen. *Gondwana Res.* 22 (2), 554–566.
- Long, X., Yuan, C., Sun, M., Xiao, W., Zhao, G., Wang, Y., Xie, L., 2010. Detrital zircon ages and Hf isotopes of the early Paleozoic flysch sequence in the Chinese Altai, NW China: new constrains on depositional age, provenance and tectonic evolution. *Tectonophysics* 480 (1), 213–231.
- Luo, Q.U.N., Zhang, C., Jiang, S.H.U., Liu, L., Liu, D., Kong, X., Liu, X., Wang, X., 2018. Partial melting of oceanic sediments in subduction zones and its contribution to the petrogenesis of peraluminous granites in the Chinese Altai. *Geol. Mag.* 1–20.
- Ma, Z.-L., 2014. Zircon U-Pb dating and Hf isotopes of pegmatites from the Kaluan mining area in the Altay, Xinjiang and their genetic relationship with the Halong

- granite. A dissertation submitted to graduate university of Chinese Academy of Sciences for the degree of Master of Philosophy, 1-70 (in Chinese with English abstract).
- Ma, X., Cai, K., Zhao, T., Bao, Z., Wang, X., Chen, M., Buslov, M.M., 2018. Devonian volcanic rocks of the southern Chinese Altai, NW China: Petrogenesis and implication for a propagating slab-window magmatism induced by ridge subduction during accretionary orogenesis. *J. Asian Earth Sci.* 160, 78–94.
- Mossakovskiy, A.A., Ruzhentsev, S.V., Samygin, S.G., Kheraskova, T.N., 1993. Central Asian fold belt: geodynamic evolution and history of formation. *Geotectonics* 6, 3–33.
- Müller, D., Rock, N.M.S., Groves, D.I., 1992. Geochemical discrimination between shoshonitic and potassic volcanic rocks in different tectonic settings: a pilot study. *Mineral. Petrol.* 46, 259–289.
- Niu, H., Sato, H., Zhang, H., Ito, J.I., Yu, X., Nagao, T., Terada, K., Zhang, Q., 2006. Juxtaposition of adakite, boninite, high-TiO₂ and low-TiO₂ basalts in the Devonian southern Altay, Xinjiang, NW China. *J. Asian Earth Sci.* 28 (4–6), 439–456.
- Pecckerillo, A., Taylor, S.R., 1976. Geochemistry of Eocene calc-alkaline volcanic rocks from the Kastamonu area, Northern Turkey. *Contrib. Miner. Petrol.* 58, 63–81.
- Rojas-Agramonte, Y., Kröner, A., Demoux, A., Xia, X., Wang, W., Donskaya, T., Liu, D., Sun, M., 2011. Detrital and xenocrystic zircon ages from Neoproterozoic to Palaeozoic arc terranes of Mongolia: significance for the origin of crustal fragments in the Central Asian Orogenic Belt. *Gondwana Res.* 19 (3), 751–763.
- Safonova, I., 2017. Juvenile versus recycled crust in the Central Asian Orogenic Belt: Implications from ocean plate stratigraphy, blueschist belts and intra-oceanic arcs. *Gondwana Res.* 47 (Supplement C), 6–27.
- Safonova, I.Y., Buslov, M.M., Iwata, K., Kokh, D.A., 2004. Fragments of Vendian-Early Carboniferous oceanic crust of the Paleo-Asian Ocean in foldbelts of the Altai-Sayan region of Central Asia: geochemistry, biostratigraphy and structural setting. *Gondwana Res.* 7 (3), 771–790.
- Safonova, I.Y., Santos, M., 2014. Accretionary complexes in the Asia-Pacific region: Tracing archives of ocean plate stratigraphy and tracking mantle plumes. *Gondwana Res.* 25 (1), 126–158.
- Scherer, E., Münker, C., Mezger, K., 2001. Calibration of the lutetium-hafnium clock. *Science* 293 (5530), 683–687.
- Schlumann, K., Paterson, S., 2011. Geodynamics: Asian continental growth. *Nat. Geosci.* 4, 827–829.
- Sengör, A.M.C., Natal'in, B.A., Burtman, V.S., 1993. Evolution of the Altai tectonic collage and Paleozoic crustal growth in Eurasia. *Nature* 364, 299–307.
- Sengör, A.M.C., Natal'in, B.A., Sunal, G. and Voo, R.v.d., 2018. The Tectonics of the Altaiids: Crustal Growth During the Construction of the Continental Lithosphere of Central Asia Between ~750 and ~130 Ma Ago. *Ann. Rev. Earth Planet. Sci.* 46(1), 439–494.
- Shand, S.J., 1943. Eruptive Rocks. Their Genesis, Composition, Classification, and Their Relation to Ore-Deposits with a Chapter on Meteorite. New York: John Wiley & Sons.
- Soejono, I., Čáp, P., Miková, J., Janoušek, V., Buriánek, D., Schulmann, K., 2018. Early Palaeozoic sedimentary record and provenance of flysch sequences in the Hovd Zone (western Mongolia): Implications for the geodynamic evolution of the Altai accretionary wedge system. *Gondwana Res.* 64, 163–183.
- Song, P., Tong, Y., Wang, T., Qin, Q., Zhang, J.J., Ning, D.X., 2017. Zircon U-Pb Ages and Genetic Evolution of Devonian Granitic Rocks in the Southeastern Chinese Altai and its Tectonic Implications: New evidence for Magmatic Evolution of Calc-alkaline-High-K Calc-alkaline-Alkaline Rocks. *Acta Geol. Sin.* 91 (1), 55–79 (in Chinese with English abstract).
- Song, P., Wang, T., Tong, Y., Zhang, J., Huang, H., Qin, Q., 2019. Contrasting deep crustal compositions between the Altai and East Junggar orogens, SW Central Asian Orogenic Belt: Evidence from zircon Hf isotopic mapping. *Lithos* 328–329, 297–311.
- Stern, C.R., 2011. Subduction erosion: rates, mechanisms, and its role in arc magmatism and the evolution of the continental crust and mantle. *Gondwana Res.* 20 (2), 284–308.
- Sun, M., Long, X., Cai, K., Jiang, Y., Wang, B., Yuan, C., Zhao, G., Xiao, W., Wu, F., 2009. Early Paleozoic ridge subduction in the Chinese Altai: insight from the abrupt change in zircon Hf isotopic compositions. *Sci. China, Ser. D Earth Sci.* 52 (9), 1345–1358.
- Sun, M., Yuan, C., Xiao, W., Long, X., Xia, X., Zhao, G., Lin, S., Wu, F., Kröner, A., 2008. Zircon U-Pb and Hf isotopic study of gneissic rocks from the Chinese Altai: progressive accretionary history in the early to middle Palaeozoic. *Chem. Geol.* 247 (3), 352–383.
- Sun, S.S., McDonough, W.F., 1989. Chemical and isotopic systematics of oceanic basalts: implications for mantle composition and processes. *Geol. Soc. Lond. Special Public. 42*, 313–345.
- Tong, L., Xu, Y.-G., Cawood, P.A., Zhou, X., Chen, Y., Liu, Z., 2014. Anticlockwise P-T evolution at ~280 Ma recorded from ultrahigh-temperature metapelitic granulite in the Chinese Altai orogenic belt, a possible link with the Tarim mantle plume? *J. Asian Earth Sci.* 94, 1–11.
- Villaseca, C., Barbero, L., Herreros, V., 1998. A re-examination of the typology of peraluminous granite types in intracontinental orogenic belts. *Trans. R. Soc. Edinburgh: Earth Sci.* 89 (2), 113–119.
- Wan, B., Xiao, W., Zhang, L., Windley, B.F., Han, C., Quinn, C.D., 2011. Contrasting styles of mineralization in the Chinese Altai and East Junggar, NW China: implications for the accretionary history of the southern Altaiids. *J. Geol. Soc.* 168 (6), 1311–1321.
- Wang, T., Hong, D.W., Jahn, B.M., Tong, Y., Wang, Y.B., Han, B.F., Wang, X.X., 2006. Timing, petrogenesis, and setting of Paleozoic synorogenic intrusions from the Altai Mountains, Northwest China: implications for the tectonic evolution of an accretionary orogen. *J. Geol.* 114 (6), 735–751.
- Wang, T., Jahn, B.M., Kovach, V.P., Tong, Y., Hong, D.W., Han, B.F., 2009a. Nd-Sr isotopic mapping of the Chinese Altai and implications for continental growth in the Central Asian Orogenic Belt. *Lithos* 110 (1), 359–372.
- Wang, W., Wei, C., Wang, T., Lou, Y., Chu, H., 2009b. Confirmation of pelitic granulite in the Altai orogen and its geological significance. *Chin. Sci. Bull.* 54 (14), 2543–2548.
- Wang, W., Wei, C., Zhang, Y., Chu, H., Zhao, Y., Liu, X., 2014a. Age and origin of sillimanite schist from the Chinese Altai metamorphic belt: implications for late Palaeozoic tectonic evolution of the Central Asian Orogenic Belt. *Int. Geol. Rev.* 56 (2), 224–236.
- Wang, Y., Long, X., Wilde, S.A., Xu, H., Sun, M., Xiao, W., Yuan, C., Cai, K., 2014b. Provenance of Early Paleozoic metasediments in the central Chinese Altai: Implications for tectonic affinity of the Altai-Mongolia terrane in the Central Asian Orogenic Belt. *Lithos* 210–211, 57–68.
- Wang, Y., Yuan, C., Long, X., Sun, M., Xiao, W., Zhao, G., Cai, K., Jiang, Y., 2011. Geochemistry, zircon U-Pb ages and Hf isotopes of the Paleozoic volcanic rocks in the northwestern Chinese Altai: petrogenesis and tectonic implications. *J. Asian Earth Sci.* 42 (5), 969–985.
- Wei, C., Clarke, G., Tian, W., Qiu, L., 2007. Transition of metamorphic series from the Kyanite-andalusite-types in the Altai orogen, Xinjiang, China: Evidence from petrography and calculated KMnFMASH and KFMASH phase relations. *Lithos* 96 (3), 353–374.
- Weinberg, R.F., Beccio, R., Farias, P., Suárez, N., Sola, A., 2018. Early Paleozoic accretionary orogenies in NW Argentina: Growth of West Gondwana. *Earth Sci. Rev.* 187, 219–247.
- Wilhem, C., Windley, B.F., Stampfli, G.M., 2012. The Altaiids of Central Asia: A tectonic and evolutionary innovative review. *Earth Sci. Rev.* 113 (3), 303–341.
- Windley, B.F., Alexeev, D., Xiao, W., Kröner, A., Badarch, G., 2007. Tectonic models for accretion of the Central Asian Orogenic Belt. *J. Geol. Soc.* 164 (1), 31–47.
- Windley, B.F., Kroener, A., Guo, J., Qu, G., Li, Y., Zhang, C., 2002. Neoproterozoic to Paleozoic Geology of the Altai Orogen, NW China: New Zircon Age Data and Tectonic Evolution. *J. Geol.* 110, 719–737.
- Wolf, M.B., Wyllie, P.J., 1994. Dehydration-melting of amphibolite at 10 kbar: the effects of temperature and time. *Contrib. Miner. Petrol.* 115, 369–383.
- Wong, K., Sun, M., Zhao, G., Yuan, C., Xiao, W., 2010. Geochemical and geochronological studies of the Alegedayi Ophiolitic Complex and its implication for the evolution of the Chinese Altai. *Gondwana Res.* 18, 438–454.
- Xiao, W., Sun, M., Santos, M., 2015a. Continental reconstruction and metallogeny of the Circum-Junggar areas and termination of the southern Central Asian Orogenic Belt. *Geosci. Front.* 6 (2), 137–140.
- Xiao, W., Windley, B., Sun, S., Li, J., Huang, B., Han, C., Yuan, C., Sun, M., Chen, H., 2015b. A Tale of Amalgamation of Three Permo-Triassic Collage Systems in Central Asia: Oroclines, Sutures, and Terminal Accretion. *Annu. Rev. Earth Planet. Sci.* 43 (1), 477–507.
- Xiao, W.J., Windley, B.F., Yuan, C., Sun, M., Han, C.M., Lin, S.F., Sun, S., 2009. Paleozoic multiple subduction-accretion processes of the southern Altaiids. *Am. J. Sci.* 309 (3), 221–250.
- Yang, T.N., Li, J.Y., Zhang, J.E., Hou, K.J., 2011. The Altai-Mongolia terrane in the Central Asian Orogenic Belt (CAOB): A peri-Gondwana one? Evidence from zircon U-Pb, Hf isotopes and REE abundance. *Precambr. Res.* 187 (1), 79–98.
- Yu, Y., Sun, M., Long, X., Li, P., Zhao, G., Kröner, A., Broussolle, A., Yang, J., 2017. Whole-rock Nd-Hf isotopic study of I-type and peraluminous granitic rocks from the Chinese Altai: Constraints on the nature of the lower crust and tectonic setting. *Gondwana Res.* 47, 131–141.
- Yuan, C., Sun, M., Xiao, W., Li, X., Chen, H., Lin, S., Xia, X., Long, X., 2007. Accretionary orogenesis of the Chinese Altai: insights from Paleozoic granitoids. *Chem. Geol.* 242 (1), 22–39.
- Yu, Y., Sun, M., Yuan, C., Zhao, G., Huang, X.-L., Rojas-Agramonte, Y., Chen, Q., 2019. Evolution of the middle Paleozoic magmatism in the Chinese Altai: Constraints on the crustal differentiation at shallow depth in the accretionary orogen. *J. Asian Earth Sci.* 175, 230–246.
- Zhang, C., Liu, L., Santos, M., Luo, Q., Zhang, X., 2017a. Sediment recycling and crustal growth in the Central Asian Orogenic Belt: Evidence from Sr-Nd-Hf isotopes and trace elements in granitoids of the Chinese Altay. *Gondwana Res.* 47 (Supplement C), 142–160.
- Zhang, J., Sun, M., Schulmann, K., Zhao, G., Wu, Q., Jiang, Y., Guy, A., Wang, Y., 2015. Distinct deformational history of two contrasting tectonic domains in the Chinese Altai: Their significance in understanding accretionary orogenic process. *J. Struct. Geol.* 73, 64–82.
- Zhang, J., Wang, J., Ding, R., 2000. Characteristics and U-Pb ages of zircon in metavolcanics from the Kangbutiebao Formation in the Altay orogeny, Xinjiang. *Reg. Geol. China* 19 (3), 281–287.
- Zhang, J., Wang, T., Tong, Y., Zhang, Z., Song, P., Zhang, L., Huang, H., Guo, L., Hou, Z., 2017b. Tracking deep ancient crustal components by xenocrystic/inherited zircons of Palaeozoic felsic igneous rocks from the Altai-East Junggar terrane and adjacent regions, western Central Asian Orogenic Belt and its tectonic significance. *Int. Geol. Rev.* 59 (16), 2021–2040.
- Zhao, G., Wang, Y., Huang, B., Dong, Y., Li, S., Zhang, G., Yu, S., 2018. Geological reconstructions of the East Asian blocks: From the breakup of Rodinia to the assembly of Pangea. *Earth Sci. Rev.* 186, 262–286.
- Zheng, C.Q., Kato, T., Enami, M., Xu, X.C., 2007. CHIME monazite ages of metasediments from the Altai orogen in northwestern China: Devonian and Permian ages of metamorphism and their significance. *Int. Geol. Rev.* 49 (4), 598–604.
- Zheng, J., Chai, F., Yang, F., 2016. The 401–409 Ma Xiaodonggou granitic intrusion: implications for understanding the Devonian Tectonics of the Northwest China Altai orogen. *Int. Geol. Rev.* 58 (5), 540–555.